Response to Reviewer 1

Laura Pan on behalf of all co-authors

We thank the reviewer for many suggestions. Please see the point-by-point responses below.

Point-by-point responses

In general, the authors have done a good job of responding to referee comments. The manuscript has been substantially revised; in fact, in some places it has been almost entirely re-written. The writing and structural flow of the manuscript have been improved. In the process of editing to address reviewer comments, the authors have articulated a new emphasis on "process-based retrieval evaluation", whereby, unlike in more traditional validation approaches, satellite measurements are assessed qualitatively through their dynamical consistency with meteorological fields (e.g., winds, GPH). The authors stress the value of the nadir sounders' dense horizontal sampling, but in my view what is probably the most important result from this paper --- the observational evidence supporting the conceptual model of the preferred ASM vertical transport pathway --- was enabled more by the ability of IASI to discriminate variability in the upper troposphere from that in the lower/middle troposphere than by its horizontal resolution.

Because of the extensive nature of the revisions, I have more comments on this draft than is typical for a re-review. However, the vast majority of them should be straightforward to address.

General comment:

I still object to the way the vertical information content of the nadir sounder measurements is characterized. IASI data may be reported on 19 surfaces, but as George et al. [2009] point out, the number of retrieval altitude levels is not representative of the vertical resolution. The statement is made (P5, L16-19): "Averaging kernels for layers centred at 13.5, 14.5, and 15.5 km are highlighted in the figure, because these layers are relevant to the analysis, which is focused on the 150 hPa pressure level. This level is contributed mostly by IASI CO product layer centred at 14.5 km and with a small fraction from the 13.5 km and 15.5 km layers." I do not see the basis for this statement in Figure 1b. Layers from ~8 to ~18 km seem to contribute almost equally to the value reported at 14.5 km. That IASI cannot discriminate between 150 and 200 hPa is also clearly demonstrated in Figure 4 and accompanying discussion. Although the authors do acknowledge that IASI has maximum sensitivity in the middle troposphere (P5, L23-25), the language they employ could be misleading to many readers, especially those who do not go through the data description subsection carefully. Figure 1b shows that it is simply NOT possible to "focus on the 150 hPa level" with IASI CO data. Thus, the authors may choose to analyze the IASI measurements reported on the 14.5 km level in the data file, but those values represent an average over a broad region of the upper troposphere and cannot be labelled "IASI CO at 150 hPa", as is done in numerous places throughout the manuscript (e.g., P6, L19; P7, L10, L13, L21, L26, L29, L32, L33; P9, L29; P10, L5, L19; P11, L28; P14, L11, L12, L15; P21, L3; P22, L2; P23, L4; P27, L1; P29, L1). A similar comment applies to IASI data "at 500 hPa" (P9, L29; P10, L7). I think it is fair to say that IASI can distinguish between the lower/middle and the upper

troposphere, and that is how the data analyzed here should be referred to, not by association with a specific pressure level.

The same comment can be made for the characterization of OMI data. It is stated (P4, L35) that the "layer 18" OMI product is "comparable to the 100 hPa level", and that the analysis focuses on "100 hPa OMI O3" data (e.g., P12, L4, L14, L33; P14, L26, L28; P32, L2, etc.). Given that the vertical resolution of OMI profiles near 100 hPa is 11-12 km [Liu et al., 2010b], such a characterization is not justified.

Although this is a significant issue, it is fundamentally a question of semantics that is easily rectified by explicitly noting that the IASI and OMI data represent averages over relatively thick (10-12 km) layers in the upper and lower/middle troposphere and appropriately labelling them as such in a consistent manner throughout the manuscript, rather than referring to them as 500, 150, or 100 hPa values.

We agree with the reviewer that this is an issue of semantics. When we refer to the IASI 150 hPa, it is the designation as a retrieval product. Same as the OMI layer 18 be comparable to 100 hPa. The specific information contributing to the product is discussed in the section on averaging kernels, in the comparisons and so on. Smoothing error is an issue for all satellite data. MLS 147 hPa CO retrieval for example, is also contributed by a thick layer of several kilometers. To further minimize any possible confusion about this, we have added specific "disclaimer" sentences at the beginning.

Note that the averaging kernels are results of model analyses and they have limitations in what they can show themselves. The importance of this work is that we show by using process understanding, we can demonstrate that the IASI retrieval over the region indeed has ~ 2 pieces of independent information, which is reflected in the independent upper tropospheric and lower/middle tropospheric variability. This approach we are demonstrating is complementing the ability of the averaging kernels. Due to the strong tradition in the satellite retrieval field, the averaging kernels may have been held to the position beyond its actual information content. We think the value of this work is to demonstrate how much more we can learn if we let our understanding of the process help us in an open-minded fashion.

Specific substantive comments:

* P3, L23: MLS O3 is not mentioned in this sentence, but the Livesey et al. [2008] validation paper cited for MLS CO also covered UTLS O3.

Modified.

* P4, L1-2: In the MLS Data Quality Document cited here, the accuracies of the v4 CO and O3 data are given as the RSS or the sum of the ppbv/ppmv and percentage uncertainties, respectively. That is, the systematic uncertainty for 147 hPa CO should be quoted as the RSS of 26 ppbv and 30%, and for 100 hPa O3 it should be quoted as the sum of 5 ppbv + 7%. The multiplicative terms are probably not negligible even for O3, and certainly not for CO in the ASM anticyclone.

In addition, it would be good to add "single-profile" in front of "precision" in these lines, since the precision is substantially improved when profiles are averaged together.

Modified.

* P6, L26-31: The issues with IASI data over elevated terrain, discussed later in the manuscript, should probably be mentioned here as well as a possible factor in explaining some of the IASI/MLS differences. In addition, it might be good to clarify that the "missing data in IASI" (L27) arise because of cloud contamination.

Modified.

* P7, L33-34: "… the IASI 150 hPa product is significantly contributed by the atmosphere at lower UT levels, including the 200 hPa range". While this is no doubt true, based on Figure 1b it seems possible that some of the features seen in the IASI upper tropospheric seasonal map could have come from even lower in the atmosphere. It would be good to show the IASI JJA map for the lower/middle troposphere in Figure 4 as well. This is done for a daily map in Figure 7, but since the presence of a systematic vertical tilt in the chemical structure of the anticyclone is being argued on the basis of these seasonal maps, a plot representing the lower layer average might be illuminating.

We do not consider the average of lower to middle troposphere here is helpful. The upper level seasonal average is dominated by the dynamics of anticyclone which is not the case in the lower level. We understand the desire of the reviewer to further quantify the smoothing error, however we do not think there is enough information to do so here. The important point in this work is that the IASI retrieval in the region can discriminate the upper tropospheric variability from that in the middle and lower troposphere.

* P8, L30: It is stated (here and in the caption to Figure 6) that daily means are calculated over the longitude range 0-220E. But the study domain was previously characterized as extending over 0-180E (P5, L6), and the Hovmoller plots only cover that hemisphere as well, so it raises the question of why the daily means are calculated over a broader region.

This is because the study region is dominated by the three Highs. When calculating anomaly, it is necessary to include part of the background outside the highs for the positive anomaly to be identified. We added a note in the text.

* P9, L12-14: A reference (Pan et al. [2016]?) would be appropriate for this mention of the modeling analysis.

Added.

* P9, L32-33: "… effective test whether the retrieval sensitivity is sufficient to resolve independent CO variability". This statement should be qualified. The comparison represents an effective test of whether IASI's sensitivity is sufficient to resolve independent upper and lower/middle tropospheric variability.

Modified.

* P11, L9-11: The weaker CO enhancement over the Tibetan Plateau is attributed to the impact of the elevated terrain on the retrieval. However, the enhancement in Fig. 9a is weak only over part of the Plateau area -- it is relatively strong around 29-30N.

The weakening here is mostly toward the altitude of enhancement. The IASI enhancement in this case ended at lower altitude and is not appearing at the 150 hPa level. A sentence is added to explain this.

* P11, L13: "the enhanced layers are centered near 150 hPa and vertically extended between 100 and 200 hPa". Again, IASI cannot really discriminate between these levels. Given the "smoothing error" in the retrieval, it is not possible to quantify the true vertical extent of this feature.

Modified.

* P11, L12-15: I am a little confused by the discussion of CO enhancement over the Western Pacific High being associated with strong easterlies in the case of Fig. 9b (though not in the case of Fig. 9d). Here and previously (P8), this feature is attributed to eastward eddy shedding, which seems inconsistent with the presence of strong easterlies. Some elaboration of this point would be helpful.

This is purely an observation, which is somewhat interesting when you look at the cross section and them together. They are on two different sides of the Tibetan High so not all eastward. We deleted the sentence since it causes unnecessary confusions here.

* P12, L8: The previous work of Park et al. [2007, Fig. 9] is described as analyzing MLS 100 hPa CO, but it would be more appropriate here (in a paragraph about O3) to say that Park et al. analyzed the MLS 100 hPa CO-O3 relationship.

Added O_3.

* P12, L10: In addition to its relatively coarse vertical resolution, it might be appropriate to mention the potential impacts of clouds and terrain on the OMI data, as discussed on P13.

This is a general statement and we prefer not to go into the details here.

* P12, L23-24: The weaker signature of in-mixing of stratospheric air in the OMI data is attributed to averaging of variable fine-scale structure in the seasonal map. But it seems to me that it is probably more related to the coarse vertical resolution of the OMI measurements, which effectively smears out the signature of this relatively shallow layer.

Modified.

* P14, L9-10: The weaker correlation between IASI CO and GPH is largely attributed to the effects of elevated terrain, specifically the Tibetan Plateau, on the retrieval. But I do not believe that the relative contribution of all possible factors was quantified in this work. Couldn't the coarser vertical resolution and cloud effects (missing data) also have played a role?

In this case we only point out the obvious that the terrain effect jumps out as the leading factor. Detailed attribution of all contributors is beyond what we can address in this work.

* P14, L12-13: "the IASI 150 hPa data include contributions from the level below". Again, this wording gives the impression that a much narrower layer is influencing the IASI measurements at 150 hPa than is actually the case.

Again, the main point is that IASI can sense the independent variability in the upper troposphere. However much the lower levels contribute, it did not change this qualitatively. We do not have information to say more about it quantitatively.

* P14, L32: It is stated that the analysis shows that IASI data have sufficient information content "to resolve upper tropospheric CO variability". I think it would be clearer and more accurate to employ wording similar to that in the abstract (P1, L24-25). I suggest something along the lines of: "to discriminate upper tropospheric CO variability from that in the lower to middle troposphere".

Modified.

* P15, L5-6: It is stated that "Although the retrieval has fewer degrees of freedom for each profile …". I think it would be clearer and more accurate to say "Although the retrieval has limited vertical resolution and is degraded over elevated terrain, …".

We have detailed these issues many times in the paper. At this point, this is a general comment contrasting the information of each profile compounded in the large number of profiles.

* P26, Figure 7: Are GFS winds at 150 hPa overlaid on both the MLS and IASI upper tropospheric CO maps? I expected the wind vectors to be the same in both panels, but close examination reveals small differences. Are the meteorological fields also gridded differently (as the satellite data are)?

The small differences are due to the 18Z versus daily mean GFS. We have updated the figure to all use daily mean.

* P29, Figure 10: Similarly, I expected the 150 hPa GPH fields (colored contours) to be identical between Figures 6 and 10, but there are small differences between them.

Same as the above. Fig. 6 has been updated to using daily average.

Minor points of clarification and suggested wording / figure changes (leaving most typos and grammar points to the journal copy-editors):

We have included all wording suggestions.

* P2, L1: I think that “demonstrate the value of” would work better here than “advocate for the use of”

* P2, L10: “composition … displays”

* P3, L18: “variabilities” --> “variability”

* P3, L21: “weak” does not seem like the right word for “resolution”; I suggest “poor” or “coarse” here instead

* P3, L27: “for using … diagnosis” --> “to use … diagnostic”

*P4, L17: delete “works of”

* P5, L9: “no IASI retrieval product once the cloud is greater than 25% in the pixel” is somewhat awkward. I think that something like “no IASI products are available if the cloud fraction in the pixel exceeds 25%” would sound better.

* P6, L20: “rational” --> “rationale”

* P7, L35: delete “are”

* P9, L23: “is almost always referred” --> “almost always refers”

* P10, L14: I think “degraded” would work better here than “weakened”

* P10, L21: “maps” --> “values”

* P10, L34: “over the Iranian mode” --> “over the Iranian Plateau”

* P11, L9-11: “weakening” --> “degrading”

* P12, L15-16: “anticyclonic flow over the ASM” would be better as “anticyclonic flow over the ASM region” or “anticyclonic flow associated with the ASM”

* P12, L17: “interception” should be “intersection”. The same comment applies to P13, L4 and P30, L5

* P13, L5: The text states that Gaussian smoothing is applied to the 1 x 1 degree maps (i.e., OMI), but the figure caption states that smoothing is applied to all maps

* P13, L14: Just to be clear, it would be good to add “in OMI O3” after “structure”

* P13, L16-17: “the weaker vertical resolution for this potentially shallow layer in OMI may contribute” --> “the coarser vertical resolution of OMI for resolving this shallow layer may contribute”

* P13, L32: “surface elevation on retrieval” --> “surface elevation on the OMI retrieval”

* P14, L4: “limb data” --> “higher vertical resolution limb data”

* P14, L9: “the season studied” --> “the 2008 JJA season studied”

* P14, L28-29: “model-based conceptual model” --> “conceptual model”

* P20, Figure 1a: the continent outlines are hard to see. Perhaps it would help to thicken the lines, or use a different color.

* P20, Figure 1b: It would be good to add a vertical line marking the zero line.

* P26, Figure 7: please either re-draw this figure so that panel (a) is at the top, as readers expect and is the case in all other multi-panel figures in this manuscript, or simply label the bottom panel as (c) and alter the references to this figure in the text accordingly.

* P26, L4: “terrains are” --> “terrain is”

* P28, Figure 9 caption: The various overlays, which presumably represent the westerly and easterly jets, tropopause height, theta surfaces, and wind vectors, all need to be defined.

Added. Thank you.

* P32, Figure 13 caption: “tropopause pressure contour” --> “tropopause pressure contour (black)”. Also, although the Tibetan Plateau is clearly marked on other figures, it is pretty hard to see here. Perhaps a different color could be used (or perhaps pink could be used for the tropopause pressure, as in Figure 11, and then black could be used for the TP).

Modified.

Response to Reviewer 2

Laura Pan on behalf of all co-authors

We thank the reviewer for many suggestions. Please see the point-by-point responses below.

I carefully read and revised the new version of the study and I apologize with the authors for the long time I eventually needed. The revised version of the manuscript by Luo et al. was greatly improved in its overall quality and clarity. The questions posed by the authors are very interesting and now more clearly expressed and investigated. However, in my opinion, the authors failed to overcome the main shortages that were pointed out during the ACP discussion phase, i.e. the lack of robustness in the adopted IASI CO profiles and how they are interpreted in the paper. I share with the authors the conviction that many interesting results are shown but these results carry the lack of possibility for the reader to discern robust patterns versus artificious (i.e., induced by the retrieval with poor sensitivity) patterns in the nadir CO (and to a lesser extent in the O3) data. I feel the authors should give more importance to having a consistent and quantified quality of the adopted data in support of their aims. In their current analysis, high and low quality results are presented under uncontrolled circumstances. I cannot therefore recommend the manuscript for publication unless these significant flaws are overcome. I report here below a number of comments that I hope the authors will consider to improve their study.

GENERAL COMMENTS

As mentioned above, in my opinion, there are major flaws in the CO data quality and the way the data are interpreted that make the whole study unreliable. These are expected because CO data are used in the analysis outside the validated range, at a single layer with no consideration of the vertical resolution and with faulty data not removed from the analysis. This was pointed out in the ACPD phase by the reviewers citing relevant literature and persists. Please see the details in the previous report. I find it interesting and see no restrictions in trying to extract more information by comparing the CO data to known processes with your aim of a processed based evaluation. But then I think the data quality needs to be kept completely under control through error and information content analysis on each individual profile considered, and through sensitivity tests showing under which conditions the profile is correctly reproducing the CO in the sounded airmasses (see e.g. Fig 10 of George et al 2015 where a bump of high CO over a thick middle tropospheric layer is completely missed in the retrieved profile). In their current version, the reader cannot understand what parts of the maps are presenting real CO details and what parts are showing retrieval artefacts. This is clearly evident in the comparison of 3 month averages of Figure 3, which removing variability show clear biases e.g. over Africa, south of the anticyclone, over the Tibetan plateau and possibly elsewhere. This is possibly an

effect of vertical displacement of the airmasses which are not correctly picked by the retrieved profiles, leading to 50-100% differences with MLS. There is no possibility to correctly place the CO at a km scale, so at times the CO will be at the right altitude and will be retrieved, other times not. The issue affects also the vertical cross sections shown in Figure 9 where clear agreement of the CO fields with dynamical fields are seen in some parts, unexplained changes are seen in other parts. How much, where and when the reader can trust the data is not evaluated in the study and this severely affects the analysis and conclusions.

I think the general idea of a processed-based evaluation of the nadir data is interesting and important. The results in the study are however presented as they are unexpectedly better than what the averaging kernels are showing. I feel the authors should reconcile the limited information content available with the results that are shown, the latter being in fair agreement with the 2 independent points expected in the troposphere. This information is barely given and then disregarded in the analysis (e.g. in Figure 9 reporting cross sections): the key robust message in my view should be how well the CO vertical profiles are interpolating on 1-km layers the two available independent points, and how well this can describe the real atmosphere. Unless this is made clear and brought forward in the analysis, the reader is wrongly induced to think there is far more information than what is available in the data. If the same figures were to be replicated using raster plots with 2 single cells as deep as the information content is (about 10 km each), then the image would change but the advances of the dense nadir sounding may still be visible and correct. Again, sensitivity tests would clearly show how the profiles respond to the real atmosphere giving the needed support to this study.

I appreciated the effort of the author to adopt the same period of time for CO and O3. However, I missed an even brief comparison of the results of the two targets. There are clear similarities in the deficiency of CO and O3 nadir data as compared to the MLS data in the region south of the anticyclone, and likely above the Tibetan plateau. MLS in these very large regions show even 100% more CO and O3 than the nadir data. These differences are shown both on seasonal averages and on daily data, and are therefore robust and need to be addressed. Also, if the nadir data over the Tibetan plateau is unreliable (as it is for CO and at least partly for O3), then it should be removed from the analysis or a detailed error map shown in couple with the absolute values.

Response to the General Comments:

We appreciate the reviewer’s concern for using satellite data carefully and the caution for unclear data quality due to limited validation. This work is very much motivated by the fact that validation opportunities are limited. To push this limitation, we explore satellite data creatively using known physical processes. We disagree with the reviewer on the statement that the data are flawed and the study is unreliable.

Although MLS is a better understood and more validated dataset, it is still incorrect to conclude that the IASI data are wrong in places the two datasets disagree. The conclusions of this study do not depend on every IASI or MLS data point on the map giving correct CO value, but rather, on how consistently both datasets show the impact of Asian monsoon dynamics. The analysis has clearly shown that both nadir data sets are useful for investigating the sub-seasonal variability of the Asian monsoon dynamics and transport. A key point is that IASI can sense the independent variability in the upper troposphere, albeit the retrievals are weighted within a broad atmospheric layer.

All satellite data are known to have "smoothing errors", which do not make the data flawed. You can find from Fig. 1b that the UTLS MLS CO retrievals are also associated with a thick layer of ~5 kilometers. The importance of this work is that we show by using process understanding that the IASI retrieval over the region indeed has important independent information in the upper tropospheric and lower/middle tropospheric. This result is not surprising, and it is consistent with and complementary to the information content analysis based on the averaging kernels and DOFS. To show this, we have included one more figure, Fig. 1c, to show that the DOFS calculated for the most important part of the study domain is distributed near 1.9-2.0, which supports the independent variability for UT and Mid-Troposphere. We think the value of this work is to demonstrate how much more we can learn if we let our understanding of the process help interpretation of the separate data sets.

As we have mentioned in the 'overview of the revisions' file in the last round of the review, CO is a tropospheric tracer and the UT CO variability is associated with both the convective uplifting of the boundary layer air and the horizontal transport driven by the anticyclone dynamics. However, O_3 is a more complicated tracer at UT. We focus on the impact of the anticyclone and tropopause structure on the O_3 mixing ratio at 100 hPa level and how MLS and OMI data show it in this study.

In any case, we view our work as a first look at these interesting questions, and as motivation for future studies. More quantitative validation and detailed attribution of all aspects of the differences between limb-viewing and nadir-viewing data are beyond what we can address in this work.

DETAILS (P=page, L=line number)

Abstract: please revise as needed

P3 L 15-17: In order to support their aims, I think the authors should underline that the same (or nearby) airmasses are sounded but with different geometries that involve crossing other portions of the atmosphere. If it were not the case, then the comparison would make no sense.

To be more accurate, the air masses sensed by the two sensors have overlap, which is more like a loaf of French bread with a pencil sticking into it. We have modified the wording to

> .. the air masses they are sensing represent very different volume and spatial extent (described in section 2).

L18-19: it is not the retrieval which is being evaluated but the retrieved data, which include the whole chain from measurement, through retrieval, to data manipulation. I suggest also to specify the evaluation is left at a qualitative level, i.e. no quantitative information is given on the goodness of this evaluation.

Our analyses include both qualitative and quantitative comparisons of the MLS, IASI and OMI data sets. It is clear that we use the retrieved data in the study, and we believe it is appropriate to refer to the method as 'process-based retrieval evaluation'.

L19-20: I do not see any effort in the manuscript to relate the information content of the data to the dynamical/chemical patterns that are described. Therefore, I feel the sentence "From the remote sensing information content point of view" should be rephrased. Unless of course an analysis of the information content of the data was introduced in parallel as suggested in the first revision and still strongly recommended.

Revised although we did include a new figure on DOFS.

L21: to me the 10-14 km vertical resolution is poor for the aims of describing vertical resolved CO tropospheric structures, rather than "relatively weak".

Modified.

L26: why is there no attempt to improve the analysis by comparing results for CO and O3? It seems straightforward to see that shortages south of the anticyclone in the nadir-limb comparison in CO are also present in O3.

See response to general comments. The CO and O_3 are analyzed independently in this work. We chose two different tracers to examine two different aspects of the ASM dynamics in this study.

P4 L8-20: the reader should be informed that the IASI CO data is used outside the validated range (which extends up to 225 hPa in Wachter 2012 and was performed on 2 partial columns) and that the use of one point of the profile at 150 hPa is equivalent to take into account a partial column about 10 km high given the available vertical resolution. I think the study would be greatly improved if these essential details were more carefully explained and dealt with throughout the paper.

225 hPa was chose as an upper limit of IASI CO data in Wachter 2012 rather than the actual validated range of IASI CO data.

We have added 'Note that these layers are referring to the product identification. The physical information for these layer products is contributed from a broad layer, as suggested by the averaging kernels.' in the revised manuscript.

L14: I think it is necessary to add that given the 0.8-2.4 DOFS, only 1 or 2 independent partial columns can be generally extracted and the vertical profiles will be based on 1 or 2 points. The 1-km vertical grid is oversampling the available information, acting as interpolation based on the 2 independent points. This is a fundamental information for the reader and I think it needs to be correctly emphasized here and in the analyses. Again, I think the manuscript would be greatly improved by showing detailed calculation of the DOFS for the horizontal maps and vertical cross sections shown in the manuscript, possibly showing better consistency with MLS when the DOFS is higher. Having this information under control would support the strategy adopted by the authors.

We have included a new figure Fig. 1c, to show the distribution of DOFS. The distribution shows that most of the profiles in the interested region have ~ 2 pieces of information. Our analysis is highly consistent with what indicated by the DOFS.

P5 L15-20/Figure 1b: the averaging kernel at 14.5 km is completely overlapped with those from nearby altitudes. What do the authors mean when writing "This level is contributed mostly by IASI CO product layer centred at 14.5 km and with a small fraction from the 13.5 km and 15.5 km layers."? Where is this information taken from? The averaging kernels are so spread that the vertical resolution (e.g. half width half maximum of the averaging kernel) is of the order 10-14 km. In fact, the plot shows that the signal at 14.5 km is almost evenly contributed by averaging kernels from 10 to 16 km and with still relevant contributions from layers below down to at least 7 km altitude. I think the sentence needs to be rephrased and the correct emphasis to what the plot is showing given here and throughout the analysis (as it is mentioned a few lines below).

To make it more clear that the IASI CO product in the UT is contributed from a broad layer, and the 14.5 km or 150 hPa are only used for product designation, we have added a few sentences:

> Note that these layers are referring to the product identification. The physical information for these layer products is contributed from a broad layer, as suggested by the averaging kernels. Fig. 1b clearly indicates that the 1-km layer products are not intended for representing independent information from each layer. To provide a perspective of retrieval information content in the study region,

we show the distribution of DOFS for IASI profiles in Figure 1c. The distribution shows that the majority of the profiles are estimated to have DOFS close to 2, which supports the aim of this study to evaluate the UT CO variability using IASI CO product.

As we have mentioned, smoothing error and limited vertical resolution is an issue for all satellite data. MLS 147 hPa CO retrieval for example, is also contributed by a thick layer of ~5 kilometers.

L28-31: I appreciated the clarity for the usability of O3 in this study.

Thanks.

P6 L6-16: Wachter et al. 2012 finds very large sensitivity variations in CO between day and night and over land/ocean, with a shift of the maximum sensitivity from the low to the middle troposphere. Maybe this is affecting part of the nadir data and could help reconciling them with MLS?

Thanks for the suggestion. We have compared IASI CO data between daytime and nighttime when we were preparing this study. The patterns are similar to each other, and both show UT variability consistent with dynamical fields.

L33-34: I would clearly state that this comparison is needed because the data is used beyond their validated range and with an approach that is not supported by the current literature.

We have clearly stated that we focus on variability. We have made quantitative comparisons beyond the past validation study.

P7 L5: typo: “is the strongest” ◊ rephrase?

Modified.

L9: it would be useful to specify how the “the vertical information content of IASI CO retrieval” led to use the 150 hPa level.

This is included in our previous responses.

L11: typo: “of THE single year 2008”

Unchanged. “a single year of 2008” is correct.

L16-19/Figure 3: Considering this is a three-month average over fairly large boxes, the agreement seems to me not so good, with a broad spread showing very large

differences in the dataset at uncontrolled times and locations: 50 ppbv of IASI CO can be associated to 30-100 ppbv of MLS CO, 50 ppbv in MLS CO can be seen as 50-100 ppbv in IASI. Indeed, the measurement and retrieval shortages in IASI have an impact on the spread and I think this should be quantified and its goodness tested. Would removing regions producing the significant difference seen in Figure 4 greatly improve the correlation shown in Figure 3 and its significance? If so, then it should be possible to isolate those regions, investigate the source of error and seek a method for keeping or rejecting nadir data.

First, it should be noted that Fig. 3 uses daily data and not seasonal averages, as clearly stated in the figure caption. The important point in this work is that the IASI retrieval in the region can discriminate the upper tropospheric variability from that in the middle and lower troposphere, and enable analysis of sub-seasonal variability of chemical distribution. We agree that improvement in the IASI retrieval is possible and necessary, but it is beyond this study.

L25-27/Figure 4: the comparison of seasonal averages should give the best results given that temporal and spatial sampling shortages are removed. The figure clearly shows that there are serious deficiencies that need to be investigated and isolated in order to support the analysis at shorter time scale. There are large differences which do not appear to have a simple and consistent interpretation, e.g. over Africa, south of the anticyclone, over the Tibetan plateau. Looking at a IASI CO map it is not possible to understand whether the data in one region is trustable or not. Since IASI CO at 150 hPa is picking signal from different layers, it is very likely that if high CO values are encountered at the wrong altitude the retrieved data may not show it. Showing maps of error and information content may help understanding why there is agreement in some regions and not in others.

The 150 hPa IASI CO data is the designation as the retrieval product, but represent a broad layer and clearly noted in the revised text. We have stated that the information is from a broad layer rather than a wrong altitude. Additional work on data validation and quality control will be useful, but that work is beyond what we focus on here.

L29-30: the blob of high CO at 120-150E in MLS at 215 hPa is very similar to that in IASI at 150 hPa. This strongly suggests IASI is picking signal from the wrong layer and there is no control on the vertical distribution as correctly shown by the averaging kernels.

This is because physical information of IASI CO is from a relative thicker layer rather than from wrong layer.

L35: typo: “likely involve”

Revised.

P8 L1-3: I agree. So, if there are regions where the data is so poor, then I suggest these data to be removed or marked somehow. But if this is the case for a certain region, how can one further trust the data at a more detailed level? I think these sentences in the text should be translated in careful selection of what is trustable and what is not.

This work is a first look at these data comparisons, and we believe it is useful to include all of the data without determining what is or is not 'trustable'.

L5-7: following the above comments, the comparison shows significant shortages in CO data that are not characterized nor explained. Further examples: the patch of high CO is at 60E in IASI while it is over India in MLS. How to explain the weak IASI CO at 30N/30E? MLS nicely fills the white contour. What about the high CO patch below 0N/30E in MLS? There is no sign of it in IASI CO.

We agree that the differences between datasets exist, but these are part of the interesting results! Further comparisons and validation work may resolve detailed differences and ascertain if retrieval improvement is possible.

P8L11-12/Figure 5: Why are the peaks in MLS CO always south of the peaks in GPH? Is it related to the tropopause interception of 100 and 105 hPa as shown for O3? A comparison of the results of the two targets may help.

Firstly, chemical distribution is not expected to be completely co-aligned with GPH fields in all situations (especially at low latitudes). Secondly, the constructed grid data of MLS is 5x5 degree which is much coarser than GFS analysis. We simply note this behavior and leave it as a topic for future study.

L29-30: possibly rephrase? E.g., a latitude band restricted to a longitude interval. The plots are for 0-180E and not for 0-220 as written.

We have added a note in the text.

Figure 6: the figure is difficult to read apart from the zero lines. Fewer color levels may help promptly identifying highs and lows. Or possibly the addition of a few contour lines? Would it be possible to extend the longitude range to 20W or so in order to capture the zero-anomaly contour line in both GPH and MLS CO?

We have revised Fig. 6 with fewer contours.

P9 L12: what model analysis are the authors referring to? Is this literature or performed within this study? Please clarify.

Reference added.

Figure 7: Indeed, IASI CO shows very interesting information but it is again difficult to understand what parts are robust and what not. For example, why would MLS pick signal along the 135E cross section at 150hPa that is not seen in IASI? The maximum contribution of an individual measurement in MLS comes from the tangent point (say 14 km altitude in this case) along the line of sight with a spread of a few hundred km, i.e. maximum +_2/3 degrees latitude. Moving 10 degrees latitude away from the tangent point, the line of sight crosses the atmosphere already 100 km higher. So, there is no possible contamination of nearby portion of the atmosphere at a distance of 10 degrees latitude and the MLS data must be trustable within their validated errors. Why is then IASI CO about 45 ppbv at 0-20 N along the 135E cross section where MLS is seeing 80 ppbv? This and other examples show IASI CO is picking signal but with no control on when it is placing it at the right location (see comments below for Figure 9). Even more, it seems various regions lead to persistent lower values as compared to MLS, pointing to physical conditions that affect the retrieval in the same way. Again, IASI CO above the Tibetan plateau seems completely wrong. I would recommend to remove known faulty data.

We agree that there are differences in horizontal distribution in UT between IASI CO and MLS CO, and we have noted that IASI CO is influenced by terrain and cloud. The different geometries also affect datasets. However, the key point is that IASI can sense independent variability in the UT, albeit within a broad vertical layer. There may be ways to improve data retrieval in the future, but that is beyond this study.

Figure 9: please add to the caption that black contour lines represent zonal winds.

Added. Thank you.

Figure 9b: I see oscillations along the longitudes with vertical plumes of low and high CO (60/100 ppbv) at 750/250 hPa between 10N to 35N. The wind field does not seem to predict those. The same in other regions and figures. On the contrary other portions seem to be in very good agreement. However, in my view, the wind field may be consistent with CO fields that are different from those shown and 50-100% changes could be easily accommodated. Therefore, it is very difficult to validate the use of nadir CO through this possible agreement with dynamical fields with no further quality control. Which parts can one trust and which not? I find it essential to support these interesting findings with a thorough analysis of the information content, error budgets and sensitivity tests on the ability of the profiles to reproduce the real data and not produce artefact. It is very well known that artefacts/oscillations can be produced by retrievals under low information content conditions, which in fact usually lead to data rejection.

The focus of our work demonstrates that IASI can sense independent CO variability in

the upper troposphere. While there is indeed some complex structure in the retrieved CO at lower levels, we have chosen not to focus on these details in our analyses.

P10 L5-8: to me the example show two independent fields can be obtained, not whether the retrieval is reproducing the two layers correctly. Nor whether the 150 hPa is unrelated to the 250 or 300 hPa level. What is the correct altitude of those high CO values?

When we refer to the IASI 150 hPa, it is the designation as a retrieval product. As responded above, we have noted in the text that the physical information for the layer products is contributed from a broad layer.

L13-17: because of the many flaws reported above, I think the comparison does not look convincing.

See previous response.

P11 L9-11: if the data is known to be of bad quality, why not removing it from the analysis?

We think it is very useful to show these limitations which help us better understand the factors limiting the preformation of our sensors.

P11 L16-19: this is likely to be the case but the study fails to have support from the missing data quality analysis: with what error? How much is real? It seems IASI CO can very likely pick strong localized CO enhancements but how it depicts them along the vertical profile is unknown. I recall George et al. 2015 Fig 10 example.

We think in this case the physical understanding of the circulation of the region is very informative.

L21-22: again the results showed IASI CO is able to pick variability, not that it is able to correctly reproduce it.

See response to General comments.

L26-27: I do not agree. The results presented in this manuscript are fairly in agreement with the limited information content calculated by the retrieval and are coupled with the several shortages that were discussed. I think this work deserves to be fully supported by a detailed quantification of the goodness of the data and retrieval sensitivity tests that show how much, when and where the profiles are correctly reproducing the sensed CO.

See response to General comments.

L28-32/Figure 10: this figure shows the limited agreement of the data with a not refined spatial and temporal reproduction by IASI CO of the real atmosphere. This does not seem to be dependent only on the Tibetan plateau faulty data. I would recommend to repeat the correlation removing the Tibetan plateau to test it.

We think it is more useful to examine what the dataset itself can show. The imperfect correlation informs the limitation of the data.

Figure 11: considering these are 3-month averages over such a broad region and that the target is the well defined O3, I think the comparison shows significant differences that need to be addressed. This is the case of Africa and the whole regions south of the anticyclone. And the Tibetan plateau as already discussed for CO. The strong disagreement south of the anticyclone was already found in CO and inter-comparison of the two targets would likely bring new insight in these shortages. Could MLS be picking stratospheric air (as seen by O3) which OMI is missing, and IASI retrieved CO be affected by this vertical displacement of stratospheric air along its line of sight? But why would MLS see more CO than IASI does?

In this study, we focus on showing what the three datasets tell us rather than how to improve them. Given the broad layer averages, we think the overall agreement in Fig. 11 is quite encouraging.

P12 L10 please revise the conclusions accordingly with the rest. This (10-14 km) is a very poor vertical resolution for resolving the troposphere in detail, I do not see how a different claim can be made.

See our response to the General comments.

L17: does this also explain why peak CO is displaced south of the highest GPH in Figure 7 and following?

Yes. They are very similar.

The list of changes for the manuscript

1. All the changes are shown in the marked-up manuscript. Please see it below.
2. We have added a new figure (Fig. 1c) and revised Figs. 6, 7, and 13.

Space-Time Variability of UTLS Chemical Distribution in the Asian Summer Monsoon Viewed by Limb and Nadir Satellite Sensors

Jiali Luo[1,2], Laura L. Pan[2], Shawn B. Honomichl[2], John W. Bergman[2,3], William J. Randel[2], Gene Francis[2], Cathy Clerbaux[4], Maya George[4], Xiong Liu[5], and Wenshou Tian[1]

[1]Key Laboratory of Semi-Arid Climate Change and College of Atmospheric Sciences, Lanzhou University, Lanzhou, China

[2] National Center for Atmospheric Research, Boulder, Colorado, USA

[3] Bay Area Environmental Research Institute, Sonoma, California, USA

[4] LATMOS/IPSL,UPMCUniversité Paris 06 Sorbonne Universités, UVSQ, CNRS, Paris, France

[5] Harvard-Smithsonian Center for Astrophysics, Cambridge, Massachusetts, USA

Correspondence to: Laura Pan (liwen@ucar.edu)

Abstract. The Asian Summer Monsoon (ASM) creates a hemispheric scale signature in trace gas distributions in the upper troposphere and lower stratosphere (UTLS). Data from satellite retrievals are the best source of information for characterizing these large-scale signatures. Measurements from the Microwave Limb Sounder (MLS), a limb viewing satellite sensor, have been the most widely used retrieval products for these types of studies. This work explores the information for the ASM influence on UTLS chemical distribution from two nadir-viewing sensors, the Infrared Atmospheric Sounding Interferometer (IASI) and the Ozone Monitoring Instrument (OMI), together with the MLS. Day-to-day changes in carbon monoxide (CO) and ozone (O_3) tracer distributions in response to dynamical variability are examined, to assess how well the data from different sensors provide useful information for studying the impact of sub-seasonal scale dynamics on chemical fields. Our result, using June-July-August of 2008 data, shows that although the MLS provides relatively sparse horizontal sampling on daily timescales, interpolated daily CO distributions show a high degree of dynamical consistency with the synoptic scale structure and variability of the anticyclone. Our analysis also shows that the IASI CO retrieval has sufficient sensitivity to produce upper tropospheric (UT) CO with variabilities independent from the lower to middle tropospheric CO. The consistency of IASI CO field with the synoptic scale anticyclone dynamical variability demonstrates that the IASI UT CO product is a physically meaningful dataset. Furthermore, IASI CO vertical cross-sections combined with the daily maps provide the first observational evidence for a model analyses-based hypothesis on the preferred ASM vertical transport location and the subsequent horizontal redistribution via east-west eddy shedding. Similarly, the OMI O_3 profile product is shown to be capable of distinguishing the tropospheric dominated air mass in the anticyclone from the stratospheric dominated background on a daily time scale, providing consistent and complementary information to the MLS. These results not only highlight the complementary information between

nadir and limb sensors, but also ~~advocate~~ demonstrate the value ~~for the use~~ of "process-based" retrieval evaluation for characterizing satellite data information content.

1 Introduction

As a prominent atmospheric circulation feature in the upper troposphere and lower stratosphere (UTLS) during boreal summer, the Asian Summer Monsoon (ASM) anticyclone's large scale dynamical behaviour has been investigated widely in recent years (e.g., Hoskins and Rodwell, 1995; Highwood and Hoskins, 1998; Zhang et al., 2002; Liu et al., 2007; Wu et al., 2015). The ASM anticyclone is bounded by the westerly jet to the north, easterly jet to the south, and this circulation is linked to enhanced air confinement (e.g., Dunkerton, 1995; Randel and Park, 2006; Garny and Randel, 2016; Fan et al., 2017). Due to the influences of deep convection and air confinement, seasonal-mean chemical composition~~s~~ within the anticyclone near the tropopause displays distinctly surface-like characteristics; boundary layer and tropospheric tracers, such as CO, H_2O, HCN, and a large set of hydrocarbons, are significantly enhanced, while O_3 as a stratospheric tracer is significantly decreased (Park et al., 2004; Li et al., 2005; Randel and Park, 2006; Park et al., 2007; Randel et al., 2010; Vernier et al., 2011; Garny and Randel, 2013). Although the ASM anticyclone is a strong and steady feature of seasonal scale circulations in UTLS, it undergoes variations on sub-seasonal timescales. These include 10-20 day east-west migrations and the associated eddy shedding (Hsu and Plumb, 2000; Popovic and Plumb, 2001; Zhang et al, 2002; Garny and Randel, 2013). Previous studies have shown that the monsoon circulation has active/break cycles that are linked to oscillations of deep convection with timescales of 10-20 and 30-60 days (e.g., Krishnamurti and Bhalme, 1976; Krishnamurti and Ardanuy, 1980; Annamalai and Slingo, 2001; Randel and Park, 2006). Zhang et al. (2002) found that the center of the anticyclone shows bimodality in its longitude location that they classify in terms of the Tibetan mode (centered at about 90° E) and the Iranian mode (centered at about 60° E), although the degree of bimodality appears dependent on the meteorological dataset (Nützel et al., 2016). A number of recent studies have shown that sub-seasonal scale dynamical processes in the ASM region may play a significant role in UTLS transport of trace gases (Yan et al., 2011; Garny and Randel, 2013; Pan et al., 2016; Vogel et al., 2016). It is evident that diagnosing intra-seasonal variability of chemical tracers in the UTLS and their interactions with dynamical fields is important for a more complete understanding of the ASM anticyclone's chemical impact.

Satellite observations provide an essential source of information in ASM UTLS-related studies. Data from limb viewing sensors, the Aura Microwave Limb Sounder (MLS), and the Atmospheric Chemistry Experiment Fourier Transform Spectrometer (ACE-FTS), in particular, are two widely used datasets for this purpose (e.g., Park et al., 2007; Randel et al., 2010). These limb sounders offer relatively high vertical resolution but have limited horizontal sampling on daily timescales. Nadir-viewing instruments, on the other hand, offer better horizontal sampling and daily coverage but have limited vertical resolution and are primarily used to study column abundances.

This study aims to examine the representation of sub-seasonal chemical variability in the ASM UTLS from limb and nadir-viewing sensors. Two specific nadir datasets we explore are CO from the Infrared Atmospheric Sounding Interferometer (IASI) and O_3 from the Ozone Monitoring Instrument (OMI). These two data sets will be examined

together with MLS CO and O_3 data, respectively. CO is a pollution tracer and is also an effective tracer of transport in the troposphere and lower stratosphere (e.g., Bowman, 2006), with a photochemical lifetime of ~2 months in troposphere (Xiao et al., 2007). O_3 is an effective transport tracer in the UTLS because of the large gradient in its mixing ratio across the tropopause and its long lifetime relative to transport time scales in the UTLS region. In the UTLS, O_3 mostly serves as a stratospheric tracer although it also has tropospheric pollution sources. Short-term variations of O_3 in the UTLS are largely linked to synoptic scale disturbances in the tropopause region (e.g., Shapiro, 1980). These satellite datasets are examined with meteorological analyses from the Global Forecasting System (GFS) to address the following questions: 1) Do these nadir viewing instruments, designed primarily for retrieving trace gas column abundance, have sufficient information to show the ASM dynamically-driven trace gas distributions and variability at UTLS levels? 2) Are the data from nadir sensors consistent with the limb-viewing data on sub-seasonal scales with respect to dynamical variability of tracers in the ASM region? 3) What can we learn from the complementary information from limb and nadir viewing instruments?

Although the IASI CO and OMI O_3 are compared with MLS CO and O_3, respectively, it is not the goal of this work to evaluate the quantitative agreement between the nadir and limb data. The difference in viewing geometries makes limb-viewing and nadir-viewing datasets fundamentally different quantities ~~because of~~since the ~~different~~ air masses they are sensing represent very different volume and spatial ~~not~~extent (described in section 2). The goal of these comparisons, therefore, is to evaluate whether data from the two types of sensors provide a consistent picture of the ASM dynamical impact on the UTLS tracer distributions and variability~~ies~~. We characterize this type of analysis as *process-based retrieval evaluation*. ~~From the remote sensing information content point of view, t~~This analysis provides a perspective of whether the high density horizontal sampling from the nadir sensors supplements information from the limb viewing sensors, despite the relatively ~~weak~~ coarse vertical resolution, in the region of strong synoptic scale horizontal dynamical variability. ~~This analysis~~This work is therefore not a validation study, but rather, aims to complement previous validation studies of the MLS CO and O_3, the IASI CO and the OMI O_3 profile product (Livesey et al., 2008; George et al., 2009; Liu et al., 2010a, 2010b; Kroon et al., 2011; De Wachter et al., 2012; Bak et al., 2013; Safieddine et al., 2016; Barret et al., 2016; Huang et al., 2017).

Although both CO and O_3 are examined in this work, the focus is on their relationship with the ASM dynamical structure. No attempt is included here ~~for~~ to use ~~using~~ tracer-tracer relationship as an additional diagnostic~~is~~ for UTLS transport. In the CO analysis, we focus on the UT variability associated with convective pumping and the horizontal redistribution by the dynamics of the anticyclone. In the O_3 analysis, we focus on the tropopause level and the sensitivity of data to the tropopause structure. Overall, we give more focus on the CO analysis.

2 Data Description

2.1 Satellite data

For limb-viewing observations, we use MLS Version 4, level 2, 147 hPa CO and 100 hPa O_3 data. MLS is a forward-looking sounder on board the Aura satellite launched in July 2004 (Waters et al., 2006). A~~-~~ccurate data descriptions of CO and O_3, including uncertainties, are given in Livesey et al, (2017). ~~The~~ Briefly, the vertical resolution of CO retrievals at 147 hPa is 5.1 km and the single profile precision is ~16 ppbv. ~~with a~~The systematic uncertainty for 147 hPa CO is the root-sum-square (RSS) of 26 ppbv and 30%~~of ~26 ppbv~~. The O_3 retrieval has a vertical resolution of 3 km at 100 hPa. The single profile precision ~~and accuracy are~~is estimated to be ~30 ppbv. The ~~and ~5 ppbv, respectively~~systematic uncertainty for 100 hPa O_3 is estimated to be 5 ppbv + 7% (Livesey et al., 2017). As a limb sounder, MLS's field of view produces a horizontal resolution of ~6 km across the track and ~300 km (570 km) along the track for O_3 (CO) at 100 hPa (147 hPa), with a relatively low daily sampling density (~240 limb scans per orbit with ~3500 profiles during both day and night). In order to make the daily output easier to interpret, daily maps are made by interpolating the output onto a regular grid.

Nadir-viewing observations of CO are obtained from IASI (level 2 data) aboard EUMETSAT's Metop satellite. IASI measures the 'thermal infrared' (TIR) spectrum emitted by the Earth-atmosphere system with twice daily near-global coverage (with 4 simultaneous pixels of 12 km diameter every 50 km), but limited vertical resolution (Clerbaux et al., 2009). The tropospheric CO product is derived from the spectra using the FORLI retrieval algorithm, which uses a single *a priori* profile and covariance matrix (Hurtmans et al., 2012; George et al., 2015). The IASI CO level 2 retrieval product is provided as mixing ratios in 19 1–km layers from surface to 19 km altitude. The retrieval information content analysis, however, shows 0.8 to 2.4 (1.5 to 2.0 at mid-latitudes) 'independent pieces of information' (or degrees of freedom for signal (DOFS); George et al. 2009). How well this information content allows IASI CO retrieval to capture upper tropospheric variability at mid-latitude and tropical latitudes is one of the foci of this study. Our analysis will complement previous ~~works of~~ validation studies, including in situ measurements from the Measurements of OZone, water vapor, carbon monoxide and nitrogen oxides by Airbus In-service airCraft (MOZAIC) project (correlations ~ 0.7; De Wachter et al., 2012), and satellite observations from the Measurements Of Pollution In The Troposphere (MOPITT) instrument (George et al., 2015). This work also aims to complement previous IASI data analyses which shows the data reproduce monthly mean large-scale features in the UTLS over the ASM region comparable to model results from GEOS-Chem (a chemical transport model coupled to meteorological analysis from the Goddard Earth Observing System GEOS-5; Barret et al., 2016).

Nadir-viewing observations of O_3 are obtained from OMI, an O_3 sounder aboard the Aura satellite that provides daily global coverage at 13 km x 24 km footprint (Levelt et al., 2006). OMI O_3 products include retrievals of both total O_3 columns and vertical profiles. In this study, we use the O_3 profile product by Liu et al. (2010b) and Huang et al. (2017). O_3 profiles are retrieved at 24 vertical layers covering the surface to ~60 km using the optimal estimation technique constrained by a monthly and zonal mean O_3 profile climatology (McPeters et al., 2007). The OMI profile

retrievals have 6.0-7.0 degrees of freedom (5.0-6.7 in the stratosphere; Liu et al., 2005; Liu et al., 2010b; Liu et al., 2010a). The distribution of the information content is sufficient to resolve the UTLS transition region in part owing to the large O_3 gradient across the tropopause, as demonstrated by a number of previous works (Pittman et al., 2009; Liu et al., 2010a; Liu et al., 2010b; Bak et al., 2013). For vertical distribution of the averaging kernels and information content, see Liu et al. (2010b). In this work, we use a level-3 product gridded to 1° longitude x 1° latitude horizontal resolution. Only the layer 18 product~~, which is comparable to the 100 hPa level,~~ (centered around 17 km which is comparable to 100 hPa pressure) is used. In the ASM anticyclone region, this layer cuts across from UT inside the anticyclone to the LS outside. OMI has known cross-track dependent biases (Liu et al., 2010a; Liu et al., 2010b). Thus the data points from view zenith angles (VZA) greater than 58° are not used in the mapping process.

To highlight the horizontal sampling density and vertical sensitivity differences between the limb viewing and nadir viewing sensors, Fig. 1 shows the geolocations of all IASI and MLS profiles and the relevant averaging kernels for the study domain (0-180° E, 10° S- 60°N) in a single day (August 1, 2008). Both daytime and night-time samplings are included. It is apparent from Fig. 1a that IASI has a much denser horizontal coverage than the MLS. Note that both datasets have data gaps: while the MLS orbit tracks are separated by ~ 20 degree longitudes, the IASI retrieval also has significant data gap each day due to the cloud coverage (no IASI ~~retrieval~~ products are available ~~once~~ if the cloud fraction in the pixel ~~is greater than~~exceeds 25% ~~in the pixel~~). The comparison of O_3 data sampling densities between OMI and MLS is not shown but it is conceptually similar to that is shown in Fig. 1a. This disparity of sampling density and its implications for representing synoptic scale variability motivates this work of exploring the utility of nadir viewing data in characterizing chemical distributions in the UTLS on daily to sub-seasonal timescales.

Figure 1b shows the vertical information distribution for both IASI and MLS UT CO retrievals. The IASI averaging kernels for the CO product in 19 layers are shown. Averaging kernels for layers centred at 13.5, 14.5, and 15.5 km are highlighted in the figure, because these layer products~~s~~ are relevant to the analysis, which is focused on the products aim to represent the ~~-~~150 hPa pressure level. This level is contributed mostly by IASI CO product layer centred at 14.5 km and with a small fraction from the 13.5 km and 15.5 km layers. The averaging kernels shown in the figures are the average of all individual profiles included in Fig. 1a. Note that these layers are referring to the product identification. The physical information for these layer products is contributed from a broad layer, as suggested by the averaging kernels. Fig. 1b clearly indicates that the 1-km layer products are not intended for representing independent information from each layer. To provide a perspective of retrieval information content in the study region, we show the distribution of DOFS for IASI profiles in Figure 1c. The distribution shows that the majority of the profiles are estimated to have DOFS close to 2, which supports the aim of this study to evaluate the UT CO variability using IASI CO product.

MLS vertical sensitivity is shown by the standard CO averaging kernels for the 215 hPa, 147 hPa and 100 hPa product (Livesey et al., 2017). Although we focus on the 147 hPa product in this analysis, 215 hPa and 100 hPa

averaging kernels are included in the figure to contrast the sensitivity distributions in the two instruments. The figure provides a perspective that IASI retrieval information content is optimized for the middle troposphere. The UT information is much weaker, maximized over a range of UT layers, and is not sharply peaked at a particular retrieval layer. In contrast, MLS information for 147 hPa shows a strong maximum near 14 km (~ 150 hPa). The figure also indicates that both the nadir and the limb viewing sensors are expected to have "smoothing errors" in the retrieval.

A similar figure for OMI is not shown, since for ozone analysis we are not focusing on independent information between the upper and lower-to-middle troposphere, rather we focus on stratospheric versus tropospheric influence in ozone distribution near the tropopause level (~100 hPa pressure level) and expect the contrast between the air mass inside and outside the anticyclone to be dominated by the tropopause structure of the region. For more complete averaging kernel discussions, see the MLS data quality document (Livesey et al., 2017), the work of George et al. (2009) for IASI data, and Liu et al. (2010b) for OMI data.

2.2 Meteorological analysis data

We use wind fields, geopotential height (GPH), tropopause height, and potential temperature (derived from temperature and pressure) from the Global Forecast System (GFS) operational analysis (a product of the National Centers for Environmental Prediction; NCEP) to diagnose the dynamical variability of the ASM anticyclone. These 6-hourly data have a horizontal resolution of 1° on 26 pressure levels (from 1000 hPa to 10 hPa) (National Centers for Environmental Prediction/National Weather Service/NOAA/U.S. Department of Commerce, 2000). Having pressure and height for the tropopause in the product, and the determination of these levels using the native GFS grid is a major strength of the product that motivated our choice (Pan and Munchak, 2011).

3 Processing daily maps

Figure 1a highlights the sampling gaps from both MLS and IASI for mapping daily CO distributions. Careful data interpolation and smoothing to fill data gaps are essential steps for producing daily maps from the available retrievals in each given day. In general, the daily representation from MLS data requires interpolation to increase the density in coverage, while the IASI (and OMI) data densities are reduced by binned averages. We have explored three interpolation algorithms, cosine smoothing, natural neighbour, and inverse distance, for mapping data. All three methods are similar, conceptually, in filling an empty cell with weighted mean of nearby observations, but the weightings are determined differently. After experimenting with various grid sizes and mapping methods, we choose to use 5° x 5° longitudes and latitudes for mapping MLS data and 3° x2° for the IASI data. The results shown in this paper are mapped using the natural neighbour method (Watson, 1992) and followed by a Gaussian smoothing. We find that these steps produce daily maps with a good balance between representing the synoptic scale variability and the information from the data in localized structures.

Figure 2 provides an example using 1 August 2008 data, where maps of retrieved MLS CO (Fig. 2a), interpolated MLS CO (Fig. 2b) at 147 hPa, and IASI CO at 150 hPa (Fig. 2c) are shown. Note we have used different color-

scales for MLS and IASI CO and the rationale is given in next section. The dynamical fields of 150 hPa GPH and the horizontal wind are superimposed for identifying the location and structure of the ASM anticyclone. Comparison of the MLS data on the orbital tracks (Fig 2a) and the interpolated map (Fig 2b) provides a useful perspective that the mapping procedure we choose highlights the large scale dynamical consistency of the CO and the flow pattern instead of the fine scale structure. Comparison of MLS (Fig. 2b) and IASI (Fig. 2c) CO maps provide additional perspective that although both datasets show CO enhancement in the region of the ASM anticyclone, the appearance and detail of the enhancement are quite different. These differences are contributed by several factors. For example, the missing data in IASI (due to cloud contamination) and the larger grid size in MLS may both contribute to the difference in the spatial pattern of the enhancement between 90°–120° E and 20°–30° N. Similarly, the filamentary structure in IASI CO near 150° E and 30° N, although hinted in the MLS orbital data, are represented differently in the MLS CO map. Additionally, IASI signal-to-noise ratio is likely degraded over the region of elevated terrain, which will be discussed in later examples. The two datasets are also obtained in slightly different sampling times, as the MLS has a 1:30 equator crossing time and the IASI orbit has a 9:30 equator crossing time. These factors need to be kept in mind when interpreting the details.

4 Comparisons of MLS and IASI CO

Although the focus of this study is to characterize chemical tracers' space-time variability and dynamical consistency, we make quantitative comparisons between the MLS and IASI CO data in this section. The comparisons focus on the consistency between the two datasets in representing CO variability in the study domain and their representation of the well-demonstrated large-scale spatial pattern associated with the ASM anticyclone on the seasonal scale. Vertical ranges of the data were chosen to optimize the overlap of information from nadir and limb viewing instruments with the vertical extent of the anticyclone. Based on the analyses of the dynamical fields and trajectory calculations, the maximum chemical confinement in the anticyclone ~~is the strongest~~ in the vertical range is between 200-100 hPa or 12 -16 km (Randel and Park, 2006), although elevated levels of tropospheric tracers in the ASM anticyclone are evident up to 68 hPa in the MLS data (Park et al., 2007). Moreover, the strongest closed circulation of the anticyclone occurs at ~14-15 km, above the main convective outflow level (~ 12 km) (Park et al., 2008). Based on this structure and the vertical information content of IASI CO retrieval (George et al., 2009), we choose to use the IASI CO mixing ratio product near the 150 hPa level and the 147 hPa MLS CO retrieval product. The June-July-August (JJA) season of a single year of 2008 is examined.

Figure 3 shows a scatterplot of IASI 150 hPa CO (selected from the nearest layer in the IASI layer product) versus MLS 147 hPa CO level-2 product. Each point represents a co-located daily average in a 10 x 6 degrees longitude-latitude bin in the study domain for all days in the JJA 2008 period. The scatterplot shows that variations of CO in the two datasets are generally consistent and correlated (r = 0.8), although the IASI CO shows a smaller range of variability than MLS (indicated by the slope of the linear fit, 0.55). The smaller variability in IASI CO is likely contributed by a weaker detection sensitivity in the upper troposphere and the use of a single a priori profile in CO retrieval (George et al., 2015).

Figure 4 shows JJA seasonal averages for (a) MLS CO at 147 hPa, (b) MLS CO average of 147 and 215 hPa products, and (c) IASI CO at 150 hPa for 2008. Note that different ranges are used in MLS and IASI color bar to adjust for the smaller range of variability in IASI CO as indicated in Fig. 3. Selected GPH contours and wind vectors at 150 hPa for the same period are shown on all three maps to indicate the seasonal mean location of the anticyclone. The chemical signature of the ASM anticyclone is evident for all three seasonal averages. The clear chemical signature indicates that, despite the relatively weak UT sensitivity, the IASI data are capable of showing the impact of the ASM circulation on UT CO. Spatially, the MLS 147 hPa and IASI 150 hPa average CO fields show noticeable differences in their horizontal locations. The IASI enhancement pattern shows an overall eastward shift relative to the MLS. There is a pattern of strong enhancement between 120° and 150° E in IASI 150 hPa average that is not clearly present in the MLS 147 hPa average. In view of the broad vertical structure in IASI averaging kernels for the UT layers, we constructed a seasonal average layer using both MLS 147 hPa and 215 hPa products (Fig. 4b), which has a region of CO enhancement very comparable to the IASI 150 hPa pattern. This result shows that, on seasonal time scales, the UT CO enhancement has an east-west tilted vertical structure, and the IASI 150 hPa product is significantly contributed by the atmosphere at lower UT levels, including the 200 hPa range. The dynamical factors that contribute to the tilted chemical structure ~~are~~ likely involve the vertical range of the anticyclone confinement and the altitudinal distributions of the easterly and westerly jets.

In addition to the weaker enhancement and the location offset, CO enhancements over the Tibetan and Iranian plateaus are largely missing in the IASI average. This is likely a result of weakened signal-to-noise ratio in the nadir sensor retrieval due to the higher surface elevation. We re-visit this issue in later sections using daily examples.

Overall, these comparisons provide quantitative and qualitative characterizations on the seasonal and the ASM regional scale variabilities represented in the IASI CO product relative to the MLS data, which has been widely used to investigate chemical tracer distributions and transport in this region (e.g., Park et al., 2007; Santee et al., 2017). We now proceed to analyse the sub-seasonal scale variability.

5 Sub-seasonal variability of ASM UT CO from MLS and IASI data

5.1 UT CO variability from MLS data

We begin our examination of daily maps in Fig. 5, which shows mixing ratios of MLS CO at 147 hPa and the dynamical fields (winds and GPH) at 150 hPa for selected days. During the time period, the dynamical evolution of the anticyclone, as indicated by the selected GPH contours, shows different phases of the east-west oscillation (Pan et al., 2016). In this sequence, the anticyclone was initially in the Tibetan mode (July 16, when the maximum of the anticyclone as represented by the GPH was located near the southern edge of the Tibetan plateau). In subsequent days the anticyclone elongates, and the center migrates westward toward the Iranian mode (July 18). As the anticyclone further elongates, the center eventually splits, and the anticyclone forms a double center (July 22), with

the two maxima located around 30°E and 80°E and a hinted 3rd center near 135°E as indicated by the wind field. During this time period, the center of maximum CO enhancement also migrated westward from south of Tibetan plateau (16 July), to around 60°E (18 July) and 30°E (22 July). Additional effect of the anticyclone elongation is the appearance of an additional CO maximum east of the Tibetan plateau, which eventually migrates eastward to western Pacific near southern Japan (see Fig. ~~7e~~7a, 26 July), similar to the configuration of 16 July (Fig. 5a). The July 16–26 time period therefore provided an example of ASM dynamical and chemical variations in a cycle of 10-20 day east-west oscillation. We refer this additional CO maximum and associated anticyclonic circulation over the region of western Pacific near Japan as the western Pacific mode, which is likely related to a system locally referred to as Bonin High (Enomoto et al., 2003).

To quantify the correlation of CO enhancement with the dynamics of the anticyclone east-west oscillation, we compare the anomaly fields of the GPH and CO through the season in Hovmöller diagrams (Figure 6). The Hovmöller diagrams are constructed by first calculating daily mean GPH and CO in the latitude band of 10°-40° N and 0°-220° E. Note we have extended the longitude range further east in this calculation to include a larger back ground. This is because the study region is dominated by three highs. Including the region outside the highs is necessary for identifying the highs as positive anomalies. The anomaly is derived for each 5° longitude bins by subtracting the daily mean. The mean correlation of the spatial (longitudinal) variability between the CO and GPH anomalies for the three-month period is 0.92. Note that the Hovmöller diagram shown in Fig. 6 is constructed using the interpolated CO field. If using the retrieved CO data only, this correlation is significantly weaker due to the sparse sampling of MLS data. As a comparison, a similar analysis using a global model shows correlation of ~ 0.7 (Pan et al., 2016).

Note that this analysis is very similar to a previous work of ASM dynamical and chemical variability in the context of eddy shedding. Using low PV air as the dynamical tracer, the correlation analyses between daily PV and MLS CO data at 370 K during one season (May-September) resulted in a spatial correlation of ~0.5 (Garny and Randel, 2013).

Figure 6 demonstrates that the UT CO distribution is closely linked to the upper tropospheric dynamical variability of the anticyclone. The dynamics of this east-west oscillation phenomenon is the focus of a number of works (e.g., Hsu and Plumb, 2000; Popovic and Plumb, 2001; Liu et al., 2007) where convective pumping of low PV air to the upper troposphere, followed by eddy shedding creates the transient behaviour of the anticyclone. The persistent low PV at the tropopause level occurs around 90°E (Popovic and Plumb, 2001; Garny and Randel, 2013), which is considered the center of the Tibetan plateau mode (Zhang et al., 2002). The low PV air propagates both westwards and eastwards. A model analysis using CO as a tracer further concludes that the vertical transport of boundary layer air predominantly occurs near the southern flank of the Tibetan plateau, and the enhanced CO over the entire anticyclone is a result of transient mixing and anticyclone confinement (Pan et al., 2016). In Fig. 6 both GPH and MLS CO shows stronger westward propagation in 10-20 periods and relatively smaller eastward propagation.

Overall, Figs. 5 and 6 show that, despite the limited horizontal sampling, MLS data provide enough information to successfully capture the day to day co-variability of CO with the dynamical fields with the help of careful mapping procedures.

5.2 CO variability associated with ASM dynamics from IASI data analyses

We begin the IASI data discussion by evaluating the information content in the IASI UT CO retrieval. Although in the literature the term "retrieval information content" ~~is~~ almost always refers~~red~~ to the DOFS calculated using forward and retrieval models, we propose an alternative way of demonstrating the information content in this work through the analyses of dynamical consistency. This type of evaluation may bring new insight into the retrieval, since it evaluates the result of the retrieval, which may vary depending on how the sensitivity represented by the DOFS is used.

Figures ~~7a~~7b ~~b~~ c show an example of daily IASI CO maps at 500 hPa and 150 hPa. The two levels are chosen to examine the dependency of the retrieval between the upper tropospheric and mid-tropospheric CO. Dynamically, these two levels have distinct flow patterns, which should have clear signatures in the CO distribution. Comparing the CO fields between these two levels and with the flow pattern at each level provide an effective test whether the retrieval sensitivity is sufficient to resolve independent upper and lower/middle tropospheric CO variability. This result complements the retrieval information content calculated from DOFS, as shown in Fig. 1c. As a reference, we have also included the MLS CO map for the same day at the 150 hPa (Fig. ~~7c~~7a).

This chosen day (26 July 2008) follows the sequence of days from Fig. 5 for MLS and Fig. 8 for IASI. Dynamically, the upper tropospheric anticyclone is in a "tri-center" phase of the east-west oscillation, following the elongation shown in Fig. 5. There are three anticyclonic centers: the strongest one over the Tibetan plateau (~ 90°E) and the second near the border of Iranian and Iraq (~ 50°E), both indicated by the maxima of GPH; The third center is over the western Pacific near 140°E, with the closed circulation indicated by the wind arrows. IASI 150 hPa CO map shows a high degree of consistency with the flow pattern at this level, and the distribution at this level does not appear to be correlated with the 500 hPa CO map. This example demonstrates the capability of IASI retrieval to produce CO distribution in the ASM upper troposphere independent from the lower to middle troposphere CO.

Figures ~~7b~~ 7a and ~~7c~~ 7b provide another case comparison between the maps based on MLS and IASI (note the different color-scales), adding to the case in Fig. 2. Although the two maps visually show different areas of "hot spots", the overall pattern of CO enhancement are very comparable if using the area greater than ~ 85 ppbv in the MLS map and that of greater than ~ 65 ppbv in the IASI map. Over the Tibetan plateau, the IASI CO map shows decreased enhancement in the high GPH center, consistent with ~~weakened~~ degraded signal-to-noise ratio due to the high terrain (marked by grey shading in Fig. ~~7a~~7c), while over the western Pacific, the IASI CO enhancement is

more intense. This comparison provides a single day example and complements the information in Fig. 4 and the associated discussions.

Figure 8 shows the IASI 150 hPa CO maps during the same period as MLS maps in Fig. 5. The overall CO enhancement patterns are very comparable to the MLS data if comparing the area of 65 ppbv or greater with MLS ~~maps~~ values 85 ppbv or greater. The IASI maps, however, shows additional finer scale structures, consistent to the flow pattern. Similar to the previous example, all three maps show the weakening of CO enhancement over the region of high elevation both over the Tibetan and Iranian plateaus. In all three cases, the IASI maps show much stronger CO enhancement over or around the western Pacific High.

Note that physically there is no reason to expect a perfect correlation between the CO maximum and the GPH maximum, since the dynamical field and the CO mixing ratios are controlled by different processes (Garny and Randel, 2013). A significant correlation at the 150 hPa reflects the strong influence of the anticyclone dynamics on the air mass and persistent boundary layer emission and convective pumping. The interesting differences between the MLS and IASI UT CO enhancement over the western Pacific, again, suggest that the IASI UT retrievals have a broad vertical sensitivity, as shown by the averaging kernels (Fig. 1b).

In addition to UT horizontal variability, IASI data provide opportunities to investigate vertical structure of CO in the monsoon region. One of the significant conclusions from a model study (Pan et al., 2016) is that the upper tropospheric CO enhancement over the Iranian ~~mode~~ Plateau is not formed by the vertical transport from the local boundary layer. Rather, it is produced by the westward shedding from the upper troposphere over the region associated with the Tibetan mode. Similar hypothesis can be made for the western Pacific enhancement. We examine the IASI CO cross-sections to search for observational evidence for verifying these hypotheses. Four examples are shown in Fig. 9. These four pressure-latitude cross-sections are selected to examine the vertical structure in the centers of the Tibetan, Iranian and Western Pacific mode. The locations of the cross-sections are marked on the maps in Figs. 7 and 8.

The cross-section in Fig. 9a is at the center of the Tibetan mode (see Fig. 8a for map). The CO enhancement in this case extends from the surface to near 14 km, with a vertical structure consistent with the flow field, i.e., the vertical structure of the enhancement is collocated with the region of strong vertical winds over northern India and the southern flank of the Tibetan plateau. Dynamically, this is identified as the ascending branch of the monsoon Hadley cell (Wang, 2006). For more discussion on the climatological flow structure in the meridional plane, see analyses in Zhang et al. (2002). This example also shows that in this region, the plateau is taking away approximately half of the atmosphere, consequently ~~weakening~~ degrading the nadir sensor's signal-to-noise ratio for retrieval, leading to a weakened CO enhancement over the plateau at higher altitude. This factor likely contributed to the difference between MLS 147 hPa and IASI 150 hPa data based maps over the plateau (see Figs. 5a and 8a).

The cross-sections in Figs. 9b and 9d are two examples of the CO enhancement over the western Pacific High. In both cases, the enhanced layers are ~~centered near 150 hPa and vertically extended between 100 and 200 hPa.~~shown in the upper troposphere. Similarly, Fig. 9c shows an example of an enhanced UT CO layer near the southern edge

of the Iranian plateau. ~~Both Fig 9b and 9c cases show that the enhancement appears to be associated with strong easterlies.~~ In all three cases (Figs. 9b-d) the wind fields indicate a change of circulation from strong vertical motion in the lower-mid troposphere to the horizontal flow dominated upper troposphere. Overall, the cross-sections support the hypothesis that the UT CO enhancement over the middle east and the western Pacific are not a result of local vertical transport but are produced by UT redistribution via westward and eastward eddy shedding.

Figure 9 not only provides observational evidence supporting the model based hypothesis on transport structure, it also provides evidence supporting the ability of the IASI retrieval to resolve independent variability in the upper tropospheric CO. Note that in each cross-section, we have also included the retrieval *a priori* profile as the left-most column. Since the IASI retrieval uses a single *a priori* profile, the left-most column on each of the four panels are identical. The UT variability shown in each cross-section is not only dynamically consistent but also independent from the lower-to middle troposphere and the *a priori* profile. The effective use of information content in the IASI retrieval is powerfully demonstrated in these cross-sections, complementing and much more enlightening than the averaging kernels shown in Fig. 1b.

Similar to Fig. 6, we show Hovmöller diagrams of daily anomaly fields for 150 hPa GPH and IASI CO for JJA 2008 (Fig. 10) to quantify the correlation in sub-seasonal variability. As expected, the weakened retrieval signal over the plateaus produced non-physical structure around 100°E longitude segment. On both the eastern and western edges, the CO anomaly shows a tendency of eastward shift relative to the GPH anomaly, a feature that is consistent with the discussion on Fig. 4. The overall correlation is 0.69.

6 UTLS O_3 analysis using MLS and OMI data

We now turn our attention to the UTLS O_3 from MLS and OMI. While CO is a boundary layer pollution tracer, O_3 in the UTLS region is foremost a transport tracer highlighting the influence of the stratosphere, although its distribution can also be affected by photochemical production. Here, the influence of monsoon convection on the UT O_3 distribution is somewhat complicated since the polluted air masses tend to have enhanced precursors for ozone production. For these reasons, we focus on analysing ozone variability at the UTLS level using 100 hPa MLS and OMI data. The large scale O_3 distribution at the 100 hPa level over the ASM region reflects the tropospheric influence on the air mass inside the anticyclone in contrast to the stratospheric influence outside. The structure of the bulging tropopause in the monsoon region (Bian et al., 2012; Pan et al., 2016) has a significant influence of the O_3 distribution at the 100 hPa level. Lower O_3 mixing ratios are expected inside the anticyclone in the layer near 100 hPa since the tropopause is at a lower pressure inside the anticyclone than it is outside in this region. Previous work analysing MLS 100 hPa CO and O_3 led to a similar conclusion (Park et al., 2007, Fig. 9). We aim to examine how well the data from MLS, which has relatively sparse horizontal sampling but better vertical resolution, and OMI, which has high density coverage horizontally but with ~~relatively~~ coarse vertical resolution, represent the correlation between the ozone field and the sub-seasonal scale dynamical variability of the tropopause in the ASM region.

6.1 Comparison of 100 hPa MLS and OMI O3 data on seasonal scale variability

Similar to the CO analysis, we first compare the two O_3 datasets on seasonal time scales. Fig~~.~~ ure 11 shows 100 hPa MLS and OMI average O_3 for JJA 2008. Also included in the figure are seasonal averages of a few selected dynamical fields for the same time period. The 100 hPa wind field is included to show the anticyclonic flow ~~over~~ associated with the ASM. The location of the anticyclone is marked by the 16.7 km GPH contour and the contours of tropopause intersec~~cep~~tion with the 100 hPa and 105 hPa pressure surfaces. The contours of the tropopause pressure and the GPH show a small south-north offset. The 100 hPa O_3 gradient change is well aligned with the tropopause contours, supporting the concept of ASM creating a tropospheric "bubble" in the otherwise stratospheric background at this level. Both the MLS and OMI based seasonal mean show low O_3 in the area of higher tropopause as expected. MLS O_3 shows a band of high O_3 near the southern edge of the anticyclone. This is a well-known dynamical structure associated with the mixing of high latitude stratospheric air driven by the anticyclonic flow (e.g., Konopka et al., 2010). This band of high O_3 appears weaker on the OMI map. The average of the finer structure with spatial variability and the limitation of the coarse vertical resolution in detecting a shallow layer may both contribute to the weaker seasonal appearance.

To evaluate the consistency in representing variability in daily data, Fig. 12 shows a scatterplot of OMI versus MLS daily grid point average O_3 on the 100 hPa in the study region over the JJA 2008 period. The grid point average is done daily in each co-located 10 x 6 degree longitude-latitude box through the study domain. This figure is similar to the CO scatterplot in Fig. 3, but the correlation between the OMI and MLS O_3 is much better with both the slope (0.94) and the correlation coefficient (0.96) near unity.

Figures 11 and 12 characterize the good overall agreement between OMI and MLS O_3 on seasonal and ASM regional scales. We now proceed to examine the daily and sub-seasonal variability represented by the two datasets.

6.2 Representation of sub-seasonal scale variability from MLS and OMI O_3

Figure 13 shows maps of MLS and OMI O_3 mixing ratios at 100 hPa and the tropopause pressure for two selected days in July 2008. Dynamical fields of the GPH and horizontal wind are superimposed on the O_3 maps. The 105 hPa tropopause contour is included in all maps. Both sets of O_3 maps exhibit the characteristic low O_3 mixing ratios inside the anticyclone. Here the 105 hPa tropopause contour appears to correlate well with the O_3 and wind field gradients. Note that the tropopause pressure here is from the GFS final analysis product, which is based on the WMO thermal tropopause definition. Since this quantity is derived from the vertical gradient and is not analysed on the pressure surface, it's intersec~~rcep~~tion with the pressure surface can appear noisy. Gaussian smoothing is applied to the 1 x 1 degree tropopause data on all maps.

In the two selected days, the dynamical structures of the anticyclone are in two different phases as discussed in relation to Figs. 5 and 8. The ASM influence at the tropopause level shows a wider longitudinal range on the 18th (approximately 20°–130° E), and it is westward migrated on the 22nd (approximately 10°–110° E) and with a double-centered structure. The OMI O_3 map on 18th shows a close correspondence with the longitudinal range of the tropopause pressure, while the MLS map shows a westward shift of the low O_3 area. The difference in horizontal sampling density is likely a contributor. On 22nd, both MLS and OMI O_3 gradients are well co-located with the

anticyclone boundary as indicated by the 105 hPa tropopause contour. The MLS O_3 structure shows a more well-defined double-centered structure. OMI map shows a smaller O_3 depression over the Tibetan plateau. We speculate that surface elevation may have contributed to the structure in OMI O_3, similar to the IASI CO discussion. The high ozone band on the southern side of the anticyclone shows a large difference between MLS and OMI, with MLS having a much wider structure. Both the coarser horizontal sampling of MLS and the ~~weaker~~ coarser vertical resolution of OMI for resolving this ~~potentially~~ shallow layer ~~in OMI~~ may contribute to this difference.

The Hovmöller diagrams in Fig. 14 examine sub-seasonal variations and the relationship between the tropopause pressure and 100 hPa O_3 field during JJA season of 2008. All three fields in the figure are dominated by the persistent location of the anticyclone as indicated by the lower tropopause pressure and of O_3 mixing ratios between 30°E and 100°E. All three Hovmöller diagrams exhibit westward propagation in 10-20 day timescales. The correlation in the variability along the longitudinal dimension is 0.90 between the tropopause pressure and MLS O_3, and 0.76 between the tropopause pressure and OMI O_3. In both cases, the interpolated fields are used to calculate the correlations. The strong correlation between the tropopause structure and O_3 supports the conceptual model that the higher tropopause over the ASM forms a region of tropospheric "bubble" above the mean level of tropical tropopause for the season. This structure enables a unique transport pathway for air masses in the "bubble" to enter the lower stratosphere via horizontal eddy shedding, bypassing the equatorial tropical tropopause (e.g., Garny and Randel, 2016; Ploeger et al., 2017).

While the two O_3 datasets provide generally consistent large scale ozone structure, there are visible differences between MLS and OMI in small-scale structures. Potential impacts of clouds on retrievals at 100 hPa is discussed in a recent OMI validation study (Huang et al., 2017). The weaker O_3 depression near 90°E is likely contributed by the impact of surface elevation on the OMI retrieval. A better understanding of the small-scale structures can benefit from validation studies using airborne measurements targeting the ASM UTLS structure.

7 Conclusions and discussions

We have examined space-time variability of chemical tracers in the UTLS associated with the ASM represented by nadir viewing (IASI and OMI) satellite instruments in comparison with a widely used limb viewing (MLS) dataset. Using CO (a boundary layer pollution tracer) and O_3 (a stratospheric tracer), we focus on the strengths and limitations of these data for representing the distribution and variability of UTLS chemical tracers in the region of the dynamically variable ASM anticyclone. We explore whether the much denser horizontal samplings of the nadir sensors provide information complementary to the higher vertical resolution limb data for the tracer daily distribution in response to synoptic scale variability.

Our CO analysis shows that, despite a relatively coarse horizontal sampling on daily timescales, interpolated MLS 147 hPa daily CO field exhibits a high degree of correlation with the dynamical variability on synoptic scales (Figs. 5 and 6). The spatial correlation between the CO anomaly and the GPH anomaly at the 150 hPa for the ASM region is 0.92 for the 2008 JJA season studied. The same correlation for IASI CO is much weaker (r = 0.69) (Fig. 10), largely due to the missing UT enhancement over the elevated surface of the Tibetan plateau. There is also an eastward shift in CO positive anomaly pattern relative to the GPH. A comparison between IASI 150 hPa CO and

the combined MLS 147 hPa and 215 hPa CO seasonal averages leads to an insight that the IASI 150 hPa data include contributions from the level below, consistent with the broad vertical structure shown in IASI averaging kernels for the UT. This comparison also shows an east-west tilt in the CO enhancement vertical structure. Quantitatively, IASI 150 hPa CO shows a consistent variability with the MLS 147 hPa product over the ASM season and region, although IASI CO has a smaller range of variability and misses the enhancement over the plateaus, likely due to the regions' elevated surface which reduces the nadir viewing sensor's signal (Figs 3 and 4). On daily to weekly time scales, IASI's data resolve finer structures in CO distribution owing to its higher horizontal sampling density. The most important complementary information is provided by IASI vertical cross-sections (Fig. 9), which provide information identifying the region of upward transport. Selected examples provided first observation evidence supporting the model-~~-~~based hypothesis that the large-~~-~~scale UT enhancement over ASM is a combined result of vertical pumping and horizontal re-distribution at UTLS level via eddy shedding (Pan et al., 2016).

In the O_3 analysis, nadir sensor data from OMI shows a good agreement with MLS O_3 at the 100 hPa level when averaged seasonally and when compared using 10 x 6 longitude-latitude grid point daily average (Figs. 11 and 12). The dynamical consistency of 100 hPa OMI O_3 on seasonal and sub-seasonal timescales demonstrates the sufficient information for the nadir viewing datasets to contribute to the ASM dynamically-driven UTLS O_3 variability. Both MLS and OMI 100 hPa O_3 variability exhibit good correlations with the tropopause pressure, supporting the ~~model based~~ conceptual model that ASM creates a tropospheric "bubble" above the season's average tropopause in the tropics (Pan et al., 2016).

The CO maps from different levels (Fig.7) and selected cross-sections (Fig.9) both provide strong evidence that IASI has sufficient information content to discriminate upper tropospheric CO variability from that in the lower to middle troposphere~~to resolve upper tropospheric CO variability~~. This result is consistent with and complementary to the model estimates of retrieval information content, which shows that the DOFS for the interested region is approximately 2 (Fig. 1c). The overall dynamical consistency found in IASI CO maps and cross-section demonstrates the value of IASI CO data for ASM transport studies. OMI 100 hPa O_3 product also shows a high degree of correlation with the MLS product, and dynamical consistency with the variability of the tropopause. Results of this study therefore demonstrate the approach of "process-based" retrieval information content evaluation. This type of evaluation is different from traditional validation studies, where the goals are focused on retrieval accuracies and precisions, and often involve quantitative comparisons with independent and better trusted data. This type of evaluation also complements the traditional information content analyses based on forward and inverse model calculations, and gives additional physical meaning to information content from data application in process studies.

Overall, our analysis demonstrates the value of high horizontal sampling density from the nadir viewing sensors in capturing the dynamical variability of UTLS tracer distributions. Although the retrieval has fewer degrees of freedom for each profile, the large number of profiles retrieved daily at finer footprints produces valuable information regarding horizontal dynamical variability. The result of this analysis, not only demonstrated the

significant role of ASM sub-seasonal scale dynamics in UTLS chemical distributions, but also bring new insight on the dynamics of the ASM through the differences of these two types of sensors.

Statement. The authors declare that they have no conflict of interest.

Acknowledgments. This work is in part J Luo's PhD research, funded by the National Science Foundation of China (41705021, 41630421 and 41575038). The work is in part conducted at the National Center for Atmospheric Research, operated by the University Corporation for Atmospheric Research under sponsorship of the United State National Science Foundation. The IASI mission is a joint mission of EUMETSAT and the Centre National d'Etudes Spatiales (CNES, France). We thank the ULB team (Daniel Hurtmans, Pierre Coheur) for the development of the FORLI-CO retrieval algorithm, and Mijeong Park for helpful discussions. We also thank three anonymous reviewers for their helpful comments and suggestions.

References

Annamalai, H., and Slingo, J. M.: Active/break cycles: diagnosis of the intraseasonal variability of the Asian Summer Monsoon, Clim. Dyn., 18, 85–102, doi:10.1007/s003820100161, 2001.

Bak, J., Liu, X., Wei, J. C., Pan, L. L., Chance, K., and Kim, J. H.: Improvement of OMI ozone profile retrievals in the upper troposphere and lower stratosphere by the use of a tropopause-based ozone profile climatology, Atmos. Meas. Tech., 6, 2239-2254, doi: 10.5194/amt-6-2239-2013, 2013.

Barret, B., Sauvage, B., Bennouna, Y., and Le Flochmoen, E.: Upper-tropospheric CO and O_3 budget during the Asian summer monsoon, Atmos. Chem. Phys., 16, 9129–9147, doi:10.5194/acp-16-9129-2016, 2016.

Bian, J., Pan, L. L., Paulik, L., Vömel, H., Chen, H., and Lu, D.: In situ water vapor and ozone measurements in Lhasa and Kunming during the Asian summer monsoon, Geophys. Res. Lett., 39, L19808, doi:10.1029/2012GL052996, 2012.

Bowman, K. P.: Transport of carbon monoxide from the tropics to the extratropics, J. Geophys. Res., 111, D02107, doi:10.1029/2005JD006137, 2006.

Clerbaux, C., Boynard, A., Clarisse, L., George, M., Hadji-Lazaro, J., Herbin, H., Hurtmans, D., Pommier, M., Razavi, A., Turquety, S., Wespes, C., and Coheur, P.-F.: Monitoring of atmospheric composition using the thermal infrared IASI/MetOp sounder, Atmos. Chem. Phys., 9, 6041–6054, doi:10.5194/acp-9-6041-2009, 2009.

De Wachter, E., Barret, B., Le Flochmoën, E., Pavelin, E., Matricardi, M., Clerbaux, C., Hadji-Lazaro, J., George, M., Hurtmans, D., Coheur, P.-F., Nedelec, P., and Cammas, J. P.: Retrieval of MetOp-A/IASI CO profiles and validation with MOZAIC data, Atmospheric Measurement Techniques, 5, 2843-2857, Atmos. Meas. Tech., 5, 2843–2857, doi:10.5194/amt-5-2843-2012, 2012.

Dunkerton, T. J.: Evidence of meridional motion in the summer lower stratosphere adjacent to monsoon regions, J. Geophys. Res., 100, D8, 16675-16688, doi:10.1029/95JD01263, 1995.

Enomoto, T., Hoskins, B. J. and Matsuda, Y. : The formation mechanism of the Bonin high in August. Q.J.R. Meteorol. Soc., 129: 157–178. doi:10.1256/qj.01.211, 2003.

Fan Q J, Bian J C, Pan L L.: Stratospheric entry point for upper-tropospheric air within the Asian summer monsoon anticyclone. Science China Earth Sciences, 60: 1685–1693, doi: 10.1007/s11430-016-9073-5, 2017

Garny, H. and Randel, W. J.: Dynamic variability of the Asian monsoon anticyclone observed in potential vorticity and correlations with tracer distributions, J. Geophys. Res. Atmos., 118, 13,421–13,433, doi:10.1002/2013JD020908, 2013.

Garny, H. and Randel, W. J.: Transport pathways from the Asian monsoon anticyclone to the stratosphere, Atmos. Chem. Phys., 16, 2703–2718, doi:10.5194/acp-16-2703-2016, 2016.

George, M., Clerbaux, C., Hurtmans, D., Turquety, S., Coheur, P. F., Pommier, M., Hadjilazaro, J., Edwards, D. P., Worden, H., Luo, M., and McMillan, W.: Carbon monoxide distributions from the IASI/METOP mission: evaluation with other space-borne remote sensors, Atmos. Chem. Phys., 9, 8317–8330, doi:10.5194/acp-9-8317-2009, 2009.

George, M., Clerbaux, C., Bouarar, I., Coheur, P.-F., Deeter, M. N., Edwards, D. P., Francis, G., Gille, J. C., Hadji-Lazaro, J., Hurtmans, D., Inness, A., Mao, D., and Worden, H. M.: An examination of the long-term CO records from MOPITT and IASI: comparison of retrieval methodology, Atmos. Meas. Tech., 8, 4313–4328, doi:10.5194/amt-8-4313-2015, 2015.

Highwood, E. and Hoskins, B.: The tropical tropopause, Q. J. Roy. Meteor. Soc., 124, 1579-1604, doi: 10.1002/qj.49712454911, 1998.

Hoskins, B. J. and Rodwell, M. J.: A model of the Asian summer monsoon. Part I: The global scale, J. Atmos. Sci., 52, 1329-1340, doi:10.1175/1520-0469(1995)052<1329:AMOTAS>2.0.CO;2, 1995.

Hsu, C. J. and Plumb, R. A.: Nonaxisymmetric Thermally Driven Circulations and Upper-Tropospheric Monsoon Dynamics, J. Atmos. Sci., 57, 1255-1276, doi:10.1175/1520-0469(2000)057<1255:NTDCAU>2.0.CO;2, 2000.

Huang, G., Liu, X., Chance, K., Yang, K., Bhartia, P. K., Cai, Z., Allaart, M., Ancellet, G., Calpini, B., Coetzee, G. J. R., Cuevas-Agulló, E., Cupeiro, M., De Backer, H., Dubey, M. K., Fuelberg, H. E., Fujiwara, M., Godin-Beekmann, S., Hall, T. J., Johnson, B., Joseph, E., Kivi, R., Kois, B., Komala, N., König-Langlo, G., Laneve, G., Leblanc, T., Marchand, M., Minschwaner, K. R., Morris, G., Newchurch, M. J., Ogino, S.-Y., Ohkawara, N., Piters, A. J. M., Posny, F., Querel, R., Scheele, R., Schmidlin, F. J., Schnell, R. C., Schrems, O., Selkirk, H., Shiotani, M., Skrivánková, P., Stübi, R., Taha, G., Tarasick, D. W., Thompson, A. M., Thouret, V., Tully, M. B., Van Malderen, R., Vömel, H., von der Gathen, P., Witte, J. C., and Yela, M.: Validation of 10-year SAO OMI Ozone Profile (PROFOZ) product using ozonesonde observations, Atmos. Meas. Tech., 10, 2455-2475, https://doi.org/10.5194/amt-10-2455-2017, 2017.

Hurtmans, D., Coheur, P. F., Wespes, C., Clarisse, L., Scharf, O., Clerbaux, C., Hadji-Lazaro, J., George, M., and Turquety, S.: FORLI radiative transfer and retrieval code for IASI, J. Quant. Spectrosc. Ra., 113, 1391–1408, doi:10.1016/j.jqsrt.2012.02.036, 2012.

Konopka, P., Grooß, J.-U., Günther, G., Ploeger, F., Pommrich, R., Müller, R., and Livesey, N.: Annual cycle of ozone at and above the tropical tropopause: Observations versus simulations with the Chemical Lagrangian Model of the Stratosphere (CLaMS), Atmos. Chem. Phys., 10, 121–132, https://doi.org/10.5194/acp-10-121-2010, 2010.

Krishnamurti, T. N. and Bhalme, H.: Oscillations of a monsoon system. Part I. Observational aspects, J. Atmos. Sci., 33, 1937-1954, doi:10.1175/1520-0469(1976)033<1937:OOAMSP>2.0.CO;2, 1976.

Krishnamurti, T. N. and Ardanuy, P.: The 10 to 20‐day westward propagating mode and "Breaks in the Monsoons", Tellus, 32, 15-26, doi:10.3402/tellusa.v32i1.10476, 1980.

Kroon, M., de Haan, J. F., Veefkind, J. P., Froidevaux, L., Wang, R., Kivi, R., and Hakkarainen, J. J.: Validation of operational ozone prodiles from the ozone monitoring instrument, J. Geophys. Res., 116, D18305, doi:10.1029/2010JD015100, 2011.

Levelt, P. F., van den Oord, G. H. J., Dobber, M. R., Malkki, A., Visser, H., de Vries, J., Stammes, P., Lundell, J. O. V., and Saari, H.: The ozone monitoring instrument, IEEE T. Geosci. Remote., 44, 1093-1101, doi:10.1109/TGRS.2006.872333, 2006.

Li, Q., Jiang, J. H., Wu, D. L., Read, W. G., Livesey, N. J., Waters, J. W., Zhang, Y., Wang, B., Filipiak, M. J., Davis, C. P., Turquety, S., Wu, S., Park, R. J., Yantosca, R. M., and Jacob, D. L.: Convective outflow of South Asian pollution: A global CTM simulation compared with EOS MLS observations, Geophys. Res. Lett., 32, L14826, doi:10.1029/2005GL022762, 2005.

Liu, X., Chance, K., Sioris, C., Spurr, R., Kurosu, T., Martin, R., and Newchurch, M.: Ozone profile and tropospheric ozone retrievals from the Global Ozone Monitoring Experiment: Algorithm description and validation, J. Geophys. Res., 110, D20307, doi:10.1029/2005JD006240, 2005.

Liu, X., Bhartia, P., Chance, K., Froidevaux, L., Spurr, R., and Kurosu, T.: Validation of Ozone Monitoring Instrument (OMI) ozone profiles and stratospheric ozone columns with Microwave Limb Sounder (MLS) measurements, Atmos. Chem. Phys., 10, 2539-2549, doi:10.5194/acp-10-2539-2010, 2010a.

Liu, X., Bhartia, P. K., Chance, K., Spurr, R. J. D., and Kurosu, T. P.: Ozone profile retrievals from the Ozone Monitoring Instrument, Atmos. Chem. Phys., 10, 2521-2537, doi:10.5194/acp-10-2521-2010, 2010b.

Liu, Y., Hoskins, B., and Blackburn, M.: Impact of Tibetan orography and heating on the summer flow over Asia, J. Meteorol. Soc. Jpn. 85, 1-19, doi:10.2151/jmsj.85B.1, 2007.

Livesey, N. J., Filipiak, M. J., Froidevaux, L., Read,W. G., Lambert, A., Santee, M. L., Jiang, J. H., Pumphrey, H. C., Waters, J. W., Cofield, R. E., Cuddy, D. T., Daffer, W. H., Drouin, B. J., Fuller, R. A., Jarnot, R. F., Jiang, Y. B., Knosp, B. W., Li, Q. B., Perun, V. S., Schwartz, M. J., Snyder, W. V., Stek, P. C., Thurstans, R. P., Wagner, P. A., Avery, M., Browell, E. V., Cammas, J.-P., Christensen, L. E., Diskin, G. S., Gao, R.-S., Jost, H.-J., Loewenstein, M., Lopez, J. D., Nedelec, P., Osterman, G. B., Sachse, G.W., and Webster, C. R.: Validation of Aura Microwave Limb Sounder O_3 and CO observations in the upper troposphere and lower stratosphere, J. Geophys. Res., 113, D15S02, doi:10.1029/2007JD008805, 2008.

Livesey, N. J., Read, W. G., Wagner, P. A., Froidevaux, L., Lambert, A., Manney, G. L., Millán Valle, L. F., Pumphrey, H. C., Santee, M. L., Schwartz, M. J., Wang, S., Fuller, R. A., Jarnot, R. F., Knosp, B. W., and Martinez,

E.: Version 4.2 level 2 data quality and description document, https://mls.jpl.nasa.gov/data/v4-2_data_quality_document.pdf, 2017.

McPeters, R. D., Labow, G. J., and Logan, J. A.: Ozone climatological profiles for satellite retrieval algorithms, J. Geophys. Res., 112, D05308, doi: 10.1029/2005jd006823, 2007.

National Centers for Environmental Prediction/National Weather Service/NOAA/U.S. Department of Commerce: NCEP FNL operational model global tropospheric analyses continuing from July 1999. [Available at 10.5065/D6M043C6 Research Data Archive at the National Center for Atmospheric Research, Computational and Information Systems Laboratory, Boulder, Colo.], 2000.

Nützel, M., Dameris, M., and Garny, H.: Movement, drivers and bimodality of the South Asian High, Atmos. Chem. Phys., 16, 14755–14774, doi:10.5194/acp-16-14755-2016, 2016.

Pan, L. L., and Munchak, L. A.: Relationship of cloud top to the tropopause and jet structure from CALIPSO data. Journal of Geophysical Research-Atmospheres, 116, 17 pp, doi:10.1029/2010JD015462, 2011.

Pan, L. L., Honomichl, S. B., Kinnison, D. E., Abalos, M., Randel, W. J., Bergman, J. W., and Bian, J.: Transport of chemical tracers from the boundary layer to stratosphere associated with the dynamics of the Asian summer monsoon, J. Geophys. Res. Atmos., 121, 14,159–14,174, doi:10.1002/2016JD025616, 2016.

Park, M., Randel, W. J., Kinnison, D. E., Garcia, R. R., and Choi, W.: Seasonal variation of methane, water vapor, and nitrogen oxides near the tropopause: Satellite observations and model simulations, J. Geophys. Res., 109, D03302, doi:10.1029/2003JD003706, 2004.

Park, M., Randel, W. J., Gettelman, A., Massie, S. T., and Jiang, J. H.: Transport above the Asian summer monsoon anticyclone inferred from Aura Microwave Limb Sounder tracers, J. Geophys. Res., 112, D16309, doi:10.1029/2006JD008294, 2007.

Park, M., Randel, W. J., Emmons, L. K., Bernath, P. F., Walker, K. A., and Boone, C. D.: Chemical isolation in the Asian monsoon anticyclone observed in Atmospheric Chemistry Experiment (ACE-FTS) data, Atmos. Chem. Phys., 8, 757-764, doi:10.5194/acp-8-757-2008, 2008.

Pittman, J. V., Pan, L. L., Wei, J. C., Irion, F. W., Liu, X., Maddy, E. S., Barnet, C. D., Chance, K., and Gao, R. S.: Evaluation of AIRS, IASI, and OMI ozone profile retrievals in the extratropical tropopause region using in situ aircraft measurements, J. Geophys. Res., 114, 24109, doi:10.1029/2009JD012493, 2009.

Ploeger, F., Konopka, P., Walker, K., and Riese, M.: Quantifying pollution transport from the Asian monsoon anticyclone into the lower stratosphere, Atmos. Chem. Phys., 17, 7055-7066, https://doi.org/10.5194/acp-17-7055-2017, 2017.

Popovic, J. M., and Plumb, R. A.: Eddy shedding from the upper-tropospheric Asian monsoon anticyclone, J. Atmos. Sci., 58, 93-104, doi:10.1175/1520-0469(2001)058<0093:esftut>2.0.co;2, 2001.

Randel, W. J., and Park, M.: Deep convective influence on the Asian summer monsoon anticyclone and associated tracer variability observed with Atmospheric Infrared Sounder (AIRS), J. Geophys. Res., 111, D12314, doi:10.1029/2005JD006490, 2006.

Randel, W. J., Park, M., Emmons, L., Kinnison, D., Bernath, P., Walker, K. A., Boone, C., and Pumphrey, H.: Asian monsoon transport of pollution to the stratosphere, Science, 328, 611-613, doi: 10.1126/science.1182274, 2010.

Safieddine, S., Boynard, A., Hao, N., Huang, F., Wang, L., Ji, D., Barret, B., Ghude, S. D., Coheur, P.-F. Hurtmans, D. , and Clerbaux, C.: Tropospheric ozone variability during the East Asian summer monsoon as observed by satellite (IASI), aircraft (MOZAIC) and ground stations, Atmos. Chem. Phys., 16, 10489–10500, doi:10.5194/acp-16-10489-2016, 2016.

Santee, M. L., Manney, G. L., Livesey, N. J., Schwartz, M. J., Neu, J. L., and Read, W. G.: A comprehensive overview of the climatological composition of the Asian summer monsoon anticyclone based on 10 years of Aura Microwave Limb Sounder measurements, J. Geophys. Res. Atmos., 122, 5491–5514, doi:10.1002/2016JD026408, 2017.

Shapiro, M. A.: Turbulent mixing within tropopause folds as a mechanism for the exchange of chemical constituents between the stratosphere and troposphere. J. Atmos. Sci., 37, 994–1004, 1980.

Vernier, J. P., Thomason, L., and Kar, J.: CALIPSO detection of an Asian tropopause aerosol layer, Geophys. Res. Lett., 38, L07804, doi:10.1029/2010GL046614, 2011.

Vogel, B., Günther, G., Müller, R., Grooß, J.-U., Afchine, A., Bozem, H., Hoor, P., Krämer, M., Müller, S., Riese, M., Rolf, C., Spelten, N., Stiller, G. P., Ungermann, J., and Zahn, A.: Long-range transport pathways of tropospheric source gases originating in Asia into the northern lower stratosphere during the Asian monsoon season 2012, Atmos. Chem. Phys., 16, 15301-15325, doi:10.5194/acp-16-15301-2016, 2016.

Wang, B.: The Asian monsoon, Springer Science & Business Media, 2006.

Waters, J. W., Froidevaux, L., Harwood, R. S., Jarnot, R. F., Pickett, H. M., Read, W. G., Siegel, P. H., Cofield, R. E., Filipiak, M. J., Flower, D. A., Holden, J. R., Lau, G. K., Livesey, N. J., Manney, G. L., Pumphrey, H. C., Santee, M. L., Wu, D. L., Cuddy, D. T., Lay, R. R., Loo, M. S., Perun, V. S., Schwartz, M. J., Stek, P. C., Thurstans, R. P., Boyles, M. A., Chandra, K. M., Chavez, M. C., Chen, G. S., Chudasama, B. V., Dodge, R., Fuller, R. A., Girard, M. A., Jiang, J. H., Jiang, Y., Knosp, B. W., Labelle, R. C., Lam, J. C., Lee, A. K., Miller, D., Oswald, J. E., Patel, N. C., Pukala, D. M., Quintero, O., Scaff, D. M., Vansnyder, W., Tope, M. C., Wagner, P. A., and Walch, M. J.: The earth observing system microwave limb sounder (EOS MLS) on the Aura satellite, IEEE Trans. Geosci. Remote. Sens., 44, 1075-1092, doi: 10.1109/TGRS.2006.873771, 2006.

Watson, D. F., Contouring: A Guide to the Analysis and Display of Spatial Data, Pergamon Press, ISBN 008040286 0, 1992.

Wu, G., He, B., Liu, Y., Bao, Q., and Ren, R.: Location and variation of the summertime upper-troposphere temperature maximum over South Asia, Clim. Dyn., 45, 2757-2774, doi:10.1007/s00382-015-2506-4, 2015.

Xiao, Y., Jacob, D. J., and Turquety, S.: Atmospheric acetylene and its relationship with CO as an indicator of air mass age, J. Geophys. Res., 112, D12305, doi:10.1029/2006JD008268, 2007.

Yan, R., Bian, J., and Fan, Q.: The Impact of the South Asia High Bimodality on the Chemical Composition of the Upper Troposphere and Lower Stratosphere, Atmos. Oceanic Sci. Lett., 4, 229–234, http://159.226.119.58/aosl/EN/Y2011/V4/I4/229, 2011.

Zhang, Q., Guoxiong, W., and Yongfu, Q.: The bimodality of the 100 hPa South Asia High and its relationship to the climate anomaly over East Asia in summer, J. Meteorol. Soc. Jpn., 80, 733–744, doi:10.2151/jmsj.80.733, 2002.

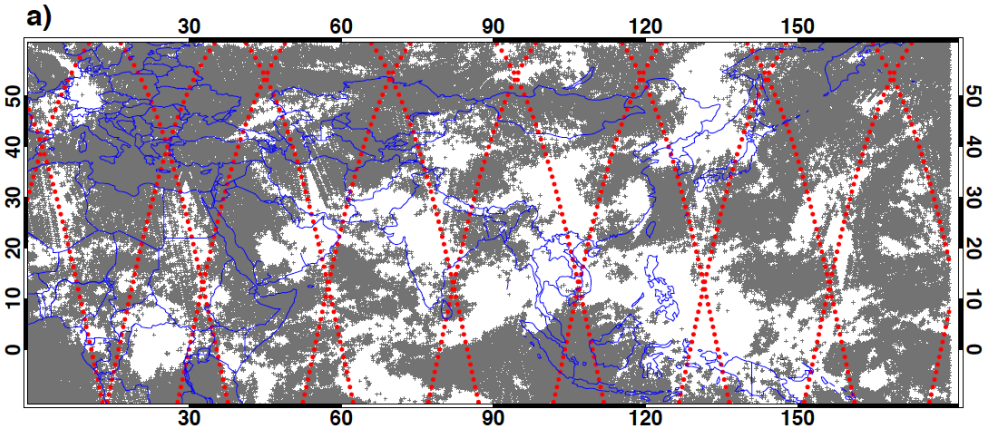
a)
30
60
90
120
150
0
10
20
30
40
50

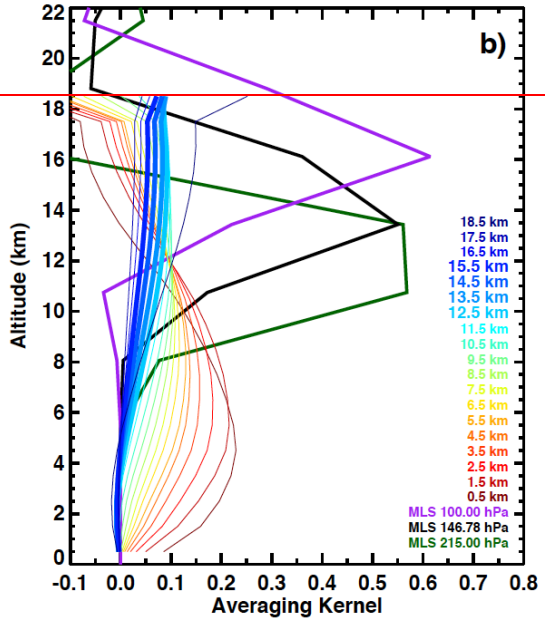
b)
Altitude (km)
Averaging Kernel
18.5 km
17.5 km
16.5 km
15.5 km
14.5 km
13.5 km
12.5 km
11.5 km
10.5 km
9.5 km
8.5 km
7.5 km
6.5 km
5.5 km
4.5 km
3.5 km
2.5 km
1.5 km
0.5 km
MLS 100.00 hPa
MLS 146.78 hPa
MLS 215.00 hPa

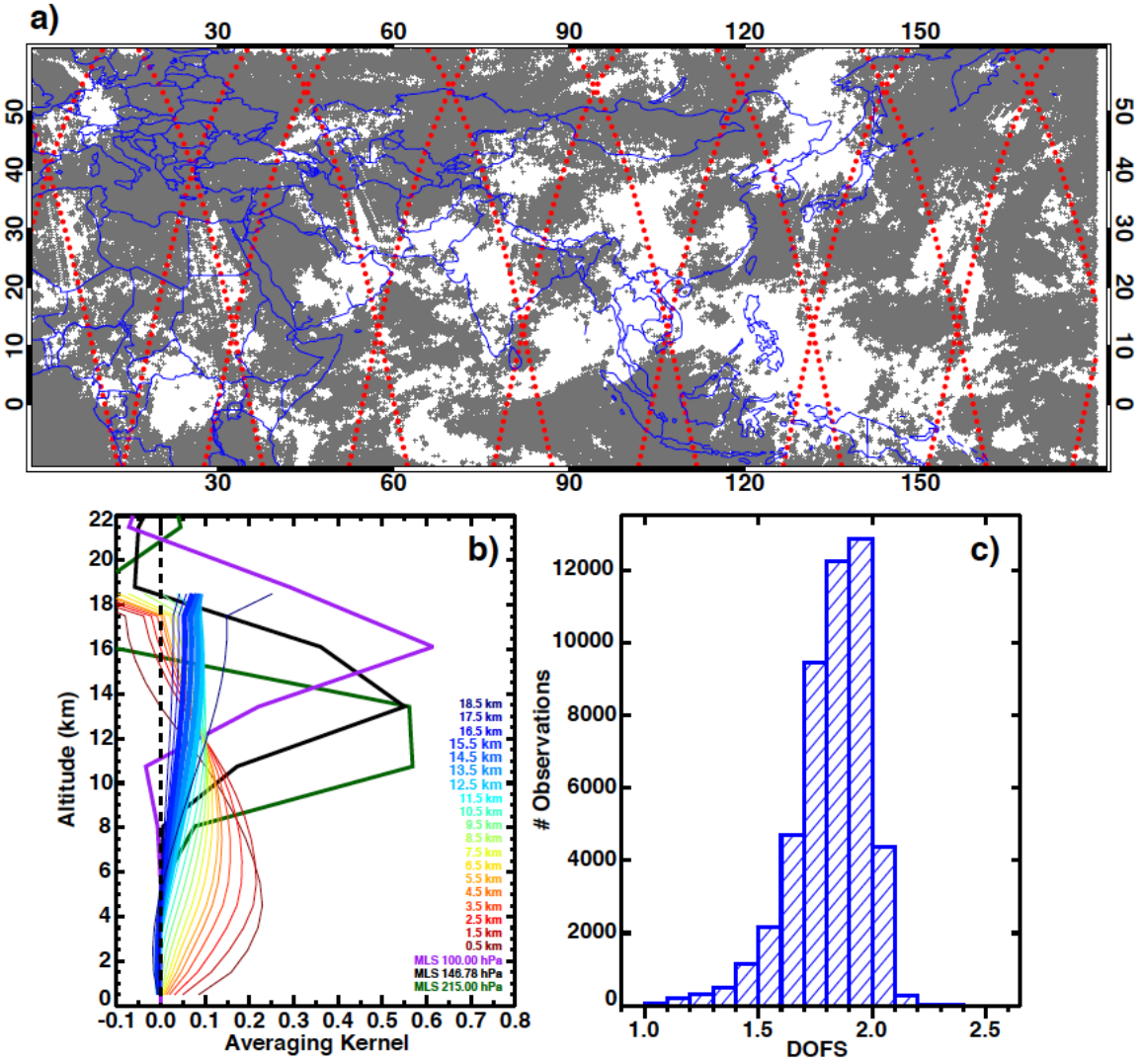

Figure 1: (a) Retrieval geolocations for IASI CO (gray crosses) and the MLS CO (red dots) on August 1, 2008 for the study domain (0°–180° E, 10°S– 60°N). Both day and night observations are included. (b) IASI averaging kernels for 19 retrieval layers from surface to 19 km, labelled by the layer-center altitudes, and the standard MLS averaging kernels for the UTLS products (215, 147, and 100 hPa). The IASI curves are the averages of all profiles from the study domain on August 1st 2008. (c) Distribution of degrees of freedom for signal (DOFS) for all IASI profiles on August 1st 2008 within [0, 40N] latitude and [40 E-150 E] longitude.

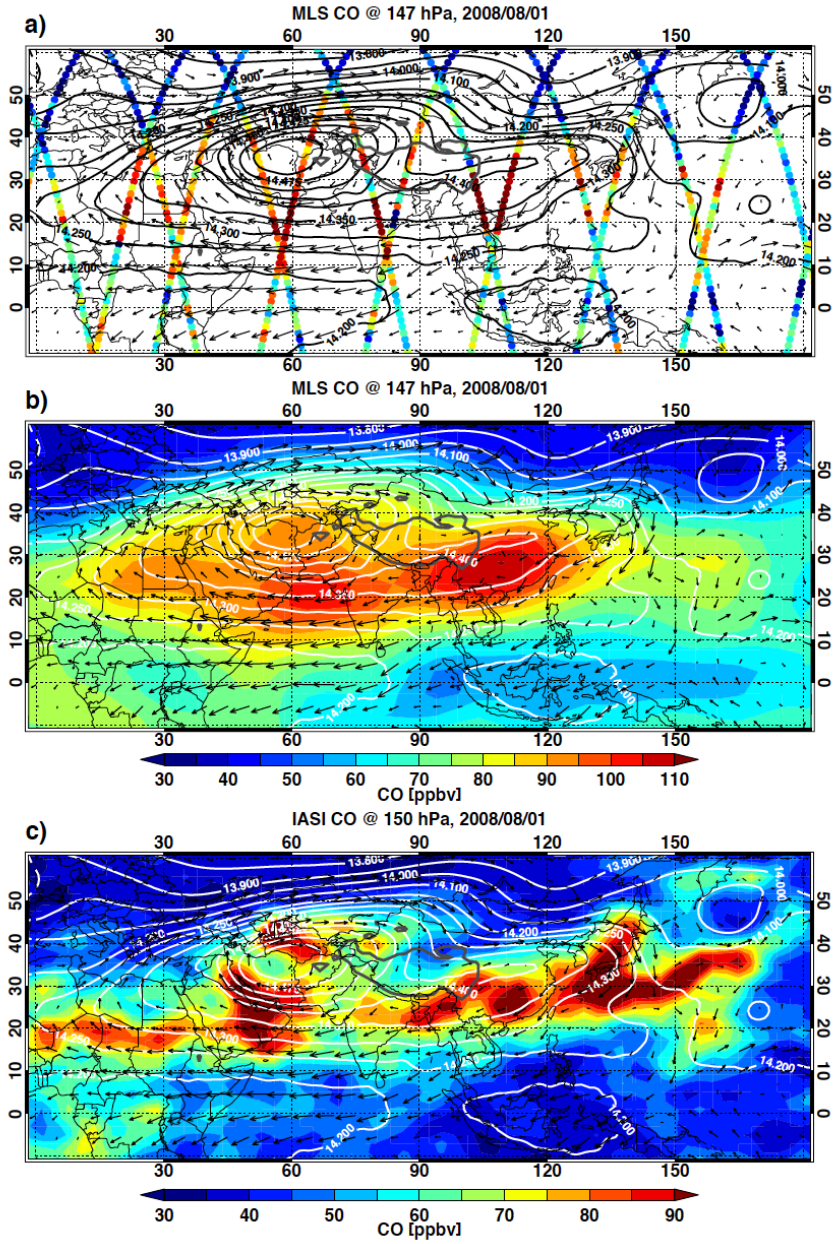

Figure 2: (a) MLS 147 hPa CO mixing ratio at retrieval geolocations on August 1, 2008, (b) the interpolated map of MLS CO and (c) the map of IASI CO at 150 hPa. The selected Geopotential Height (GPH) contours (white) and horizontal winds (black arrows) at 150 hPa are superimposed. The MLS CO map is made with 5°x5° longitude and latitude grids. The IASI CO map is made using 3°x2° grids. Both are interpolated using the natural neighbor algorithm (Watson, 1992).

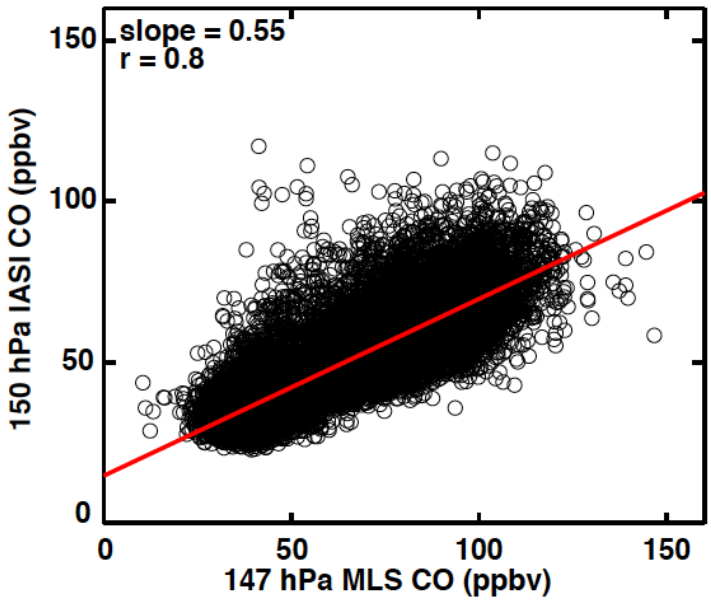

Figure 3: Scatterplot of IASI CO mixing ratio at 150 hPa versus MLS CO at 147 hPa for June, July, and August (JJA), 2008. Each data point represents a daily average of CO level-2 data from IASI and MLS in the same 10 x 6 degree longitude-latitude box in the study domain. The red line shows a linear fit. Correlation and slope for the linear fit are given in the upper left corner of the panel.

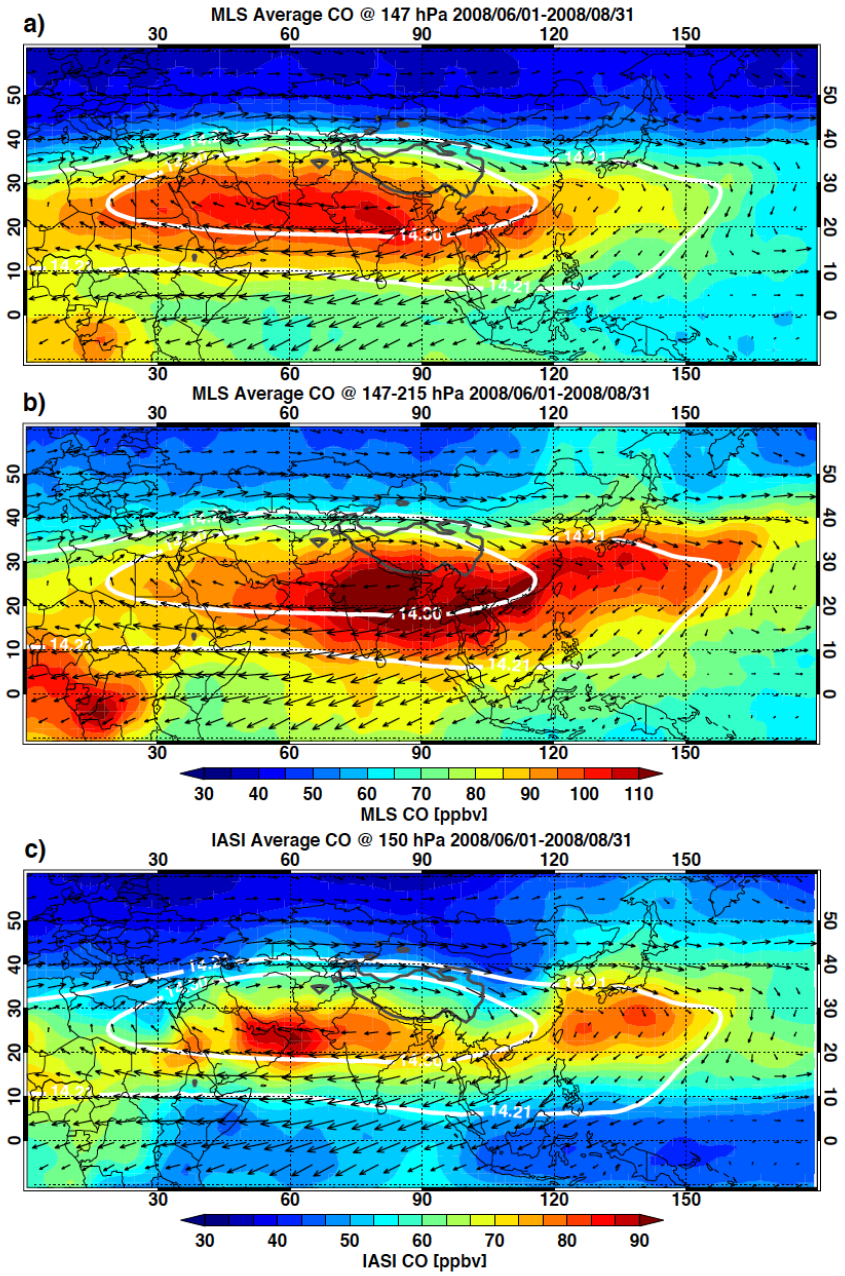

Figure 4: JJA 2008 seasonal average CO mixing ratio for (a) MLS at 147 hPa, (b) MLS 147 and 215 hPa average, and (c) IASI at 150 hPa. Superimposed white contours are the14.3 km and 14.2 km GPH (from GFS analysis) at 150 hPa. Note that the color scales for IASI and MLS CO are different. Both MLS and IASI are 2° × 2° longitude-latitude binned averages.

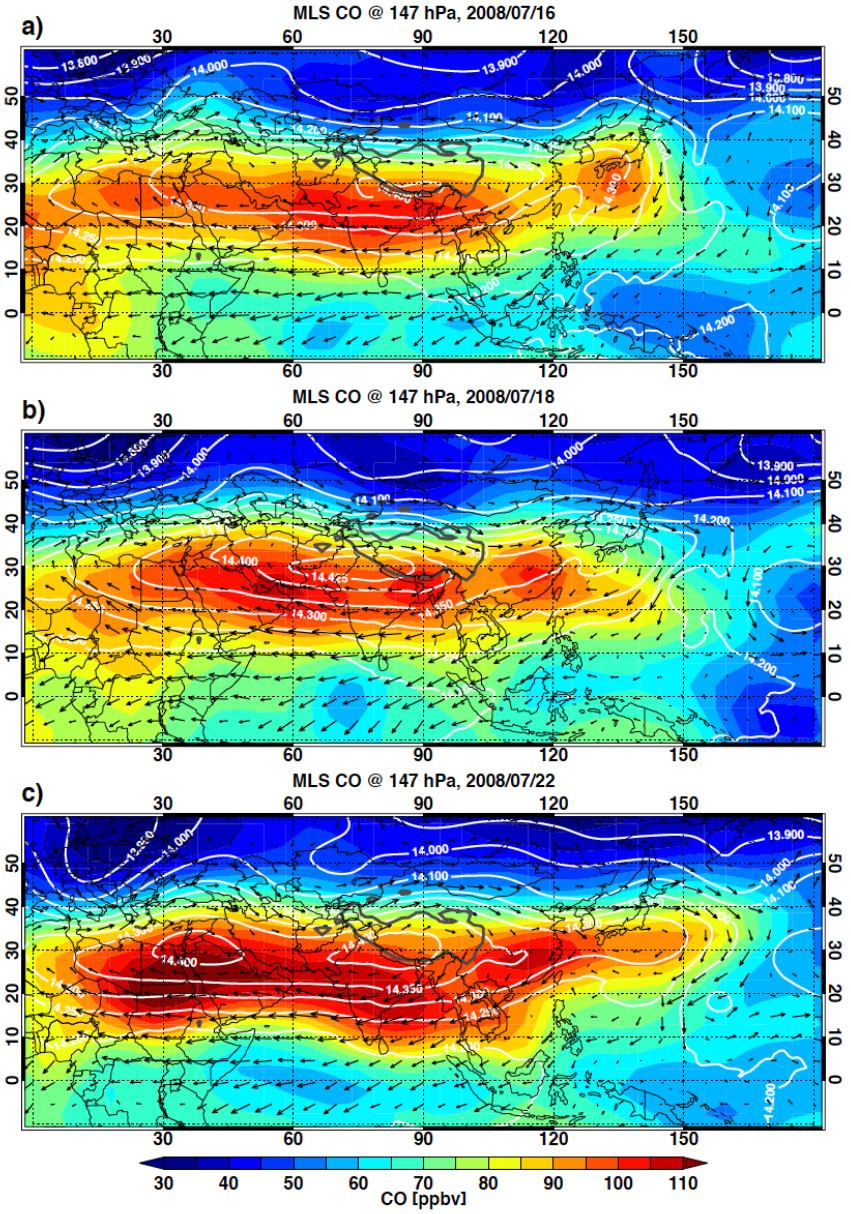

Figure 5: Daily maps of MLS CO mixing ratio at 147 hPa (color shading) on (a) July 16, (b) July 18, (c) July 22 2008. Dynamical fields of GPH (white contours) and horizontal winds (black arrows) are superimposed. Maps are interpolated using natural neighbor algorithm (Watson, 1992) to 5°x5° longitude-latitude grids. The location of the Tibetan plateau (using 3 km elevation) is also shown in the maps (thick gray).

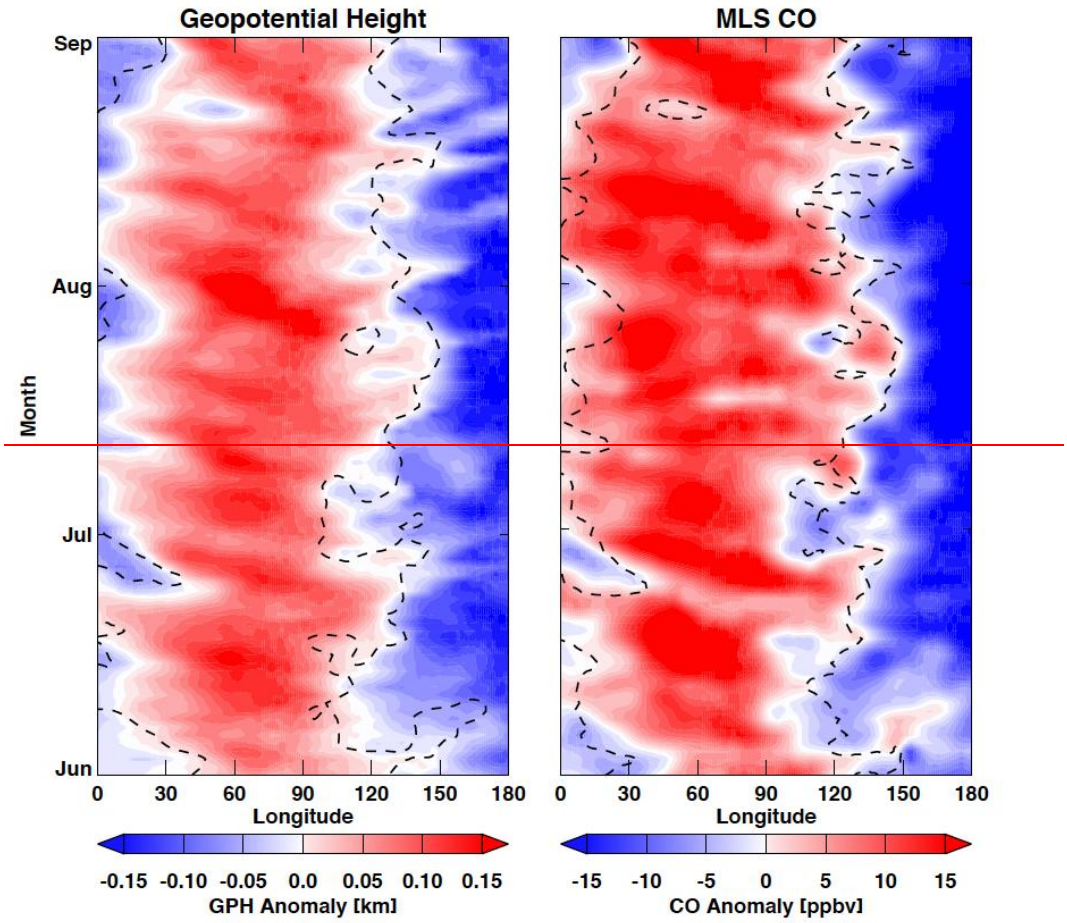
Geopotential Height
MLS CO
Sep
Aug
Jul
Jun
Month
0 30 60 90 120 150 180
Longitude
-0.15 -0.10 -0.05 0.0 0.05 0.10 0.15
GPH Anomaly [km]
-15 -10 -5 0 5 10 15
CO Anomaly [ppbv]

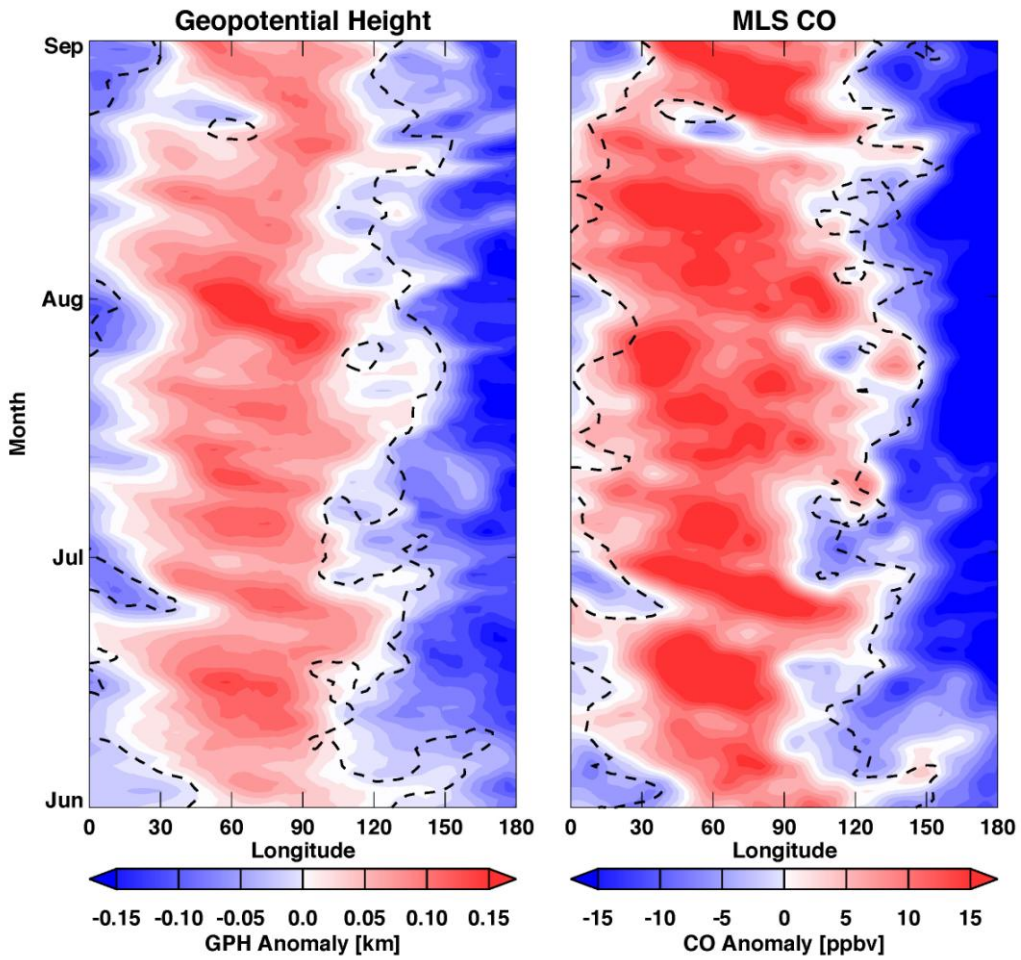

Figure 6: Hovmöller diagrams of the 150 hPa GPH and 147 hPa MLS CO anomaly for JJA 2008. The anomalies are calculated with respect to daily means over the latitude band 10°–40° N and longitude range 0°– 220°E, in 5° longitude bins. The dashed line in each panel indicates the location of the mean (zero anomaly) of the opposite field. The Pearson's correlation of the two fields for the 3-month period is 0.92.

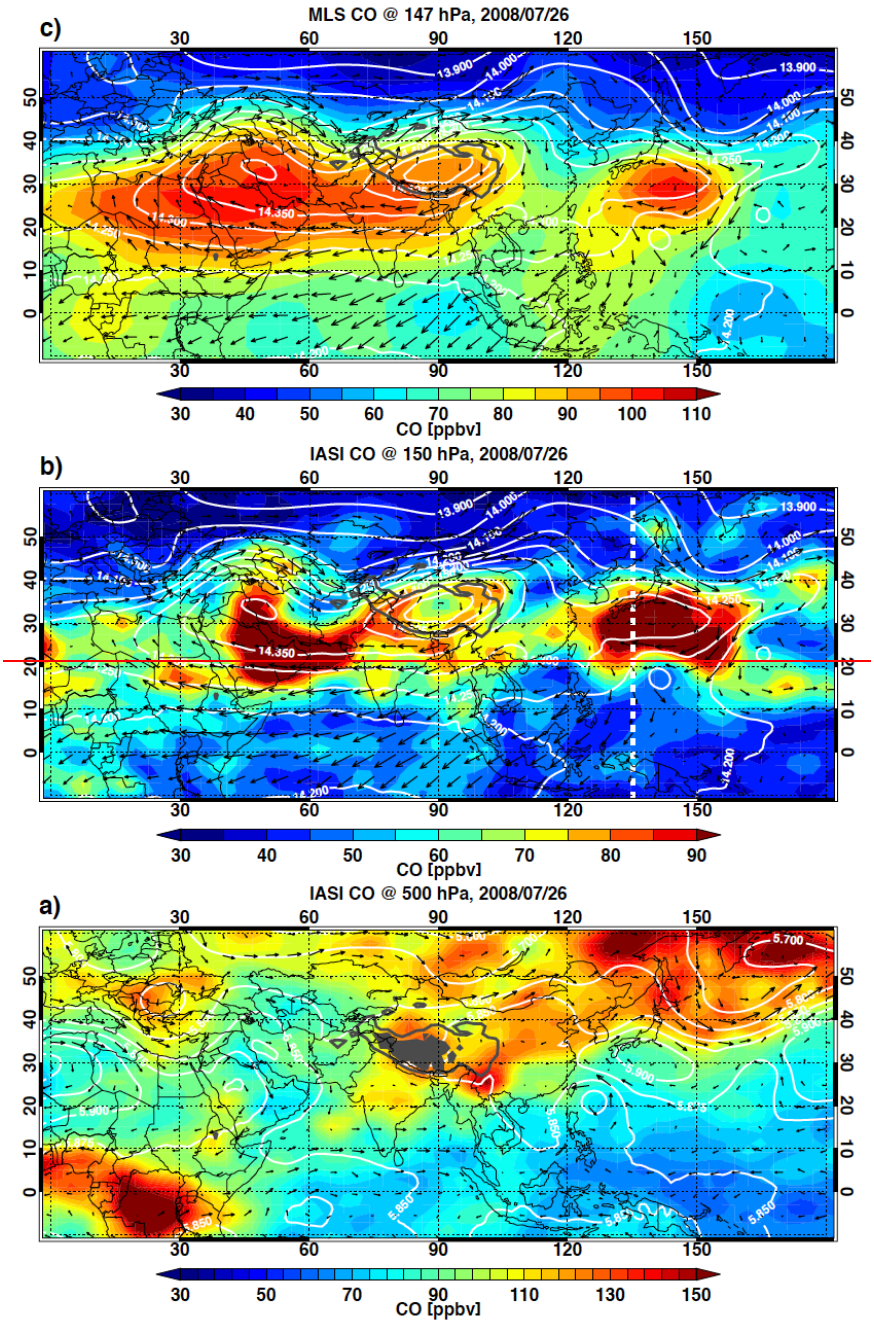
c)
MLS CO @ 147 hPa, 2008/07/26
CO [ppbv]
b)
IASI CO @ 150 hPa, 2008/07/26
CO [ppbv]
a)
IASI CO @ 500 hPa, 2008/07/26
CO [ppbv]

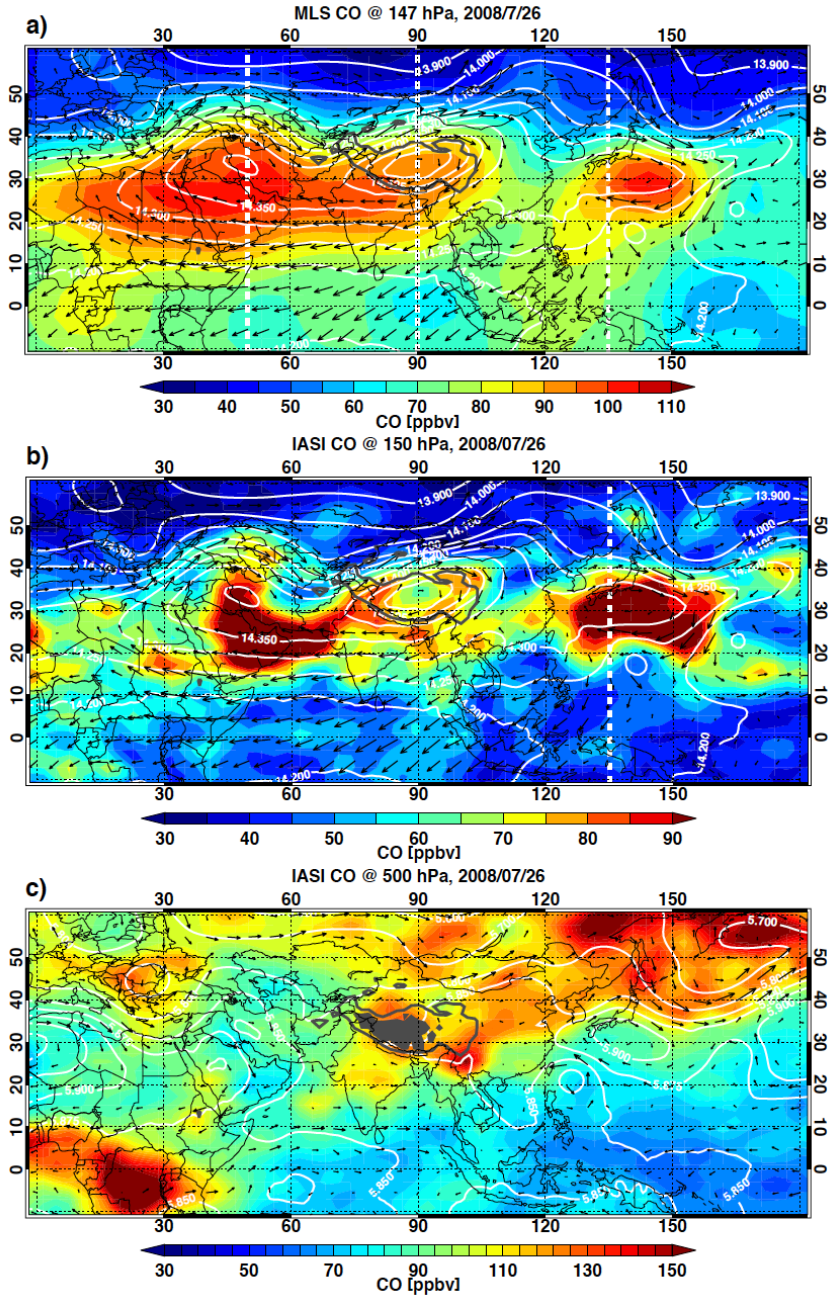

Figure 7: IASI CO at (a) 500 hPa, (b) 150 hPa levels and (c) MLS CO 147 hPa product for a selected day (26 July 2008). Dynamical fields of GPH (white contours) and horizontal winds (black arrows) for the corresponding levels are superimposed. Elevated terrain~~s~~ ~~are~~ is indicated by gray shadings for the 500 hPa map in (a). The location of the Tibetan plateau (using 3 km elevation) is also shown in the maps (thick gray line). The dashed white line in (b) marks the location of the cross-section shown in Fig. 9d.

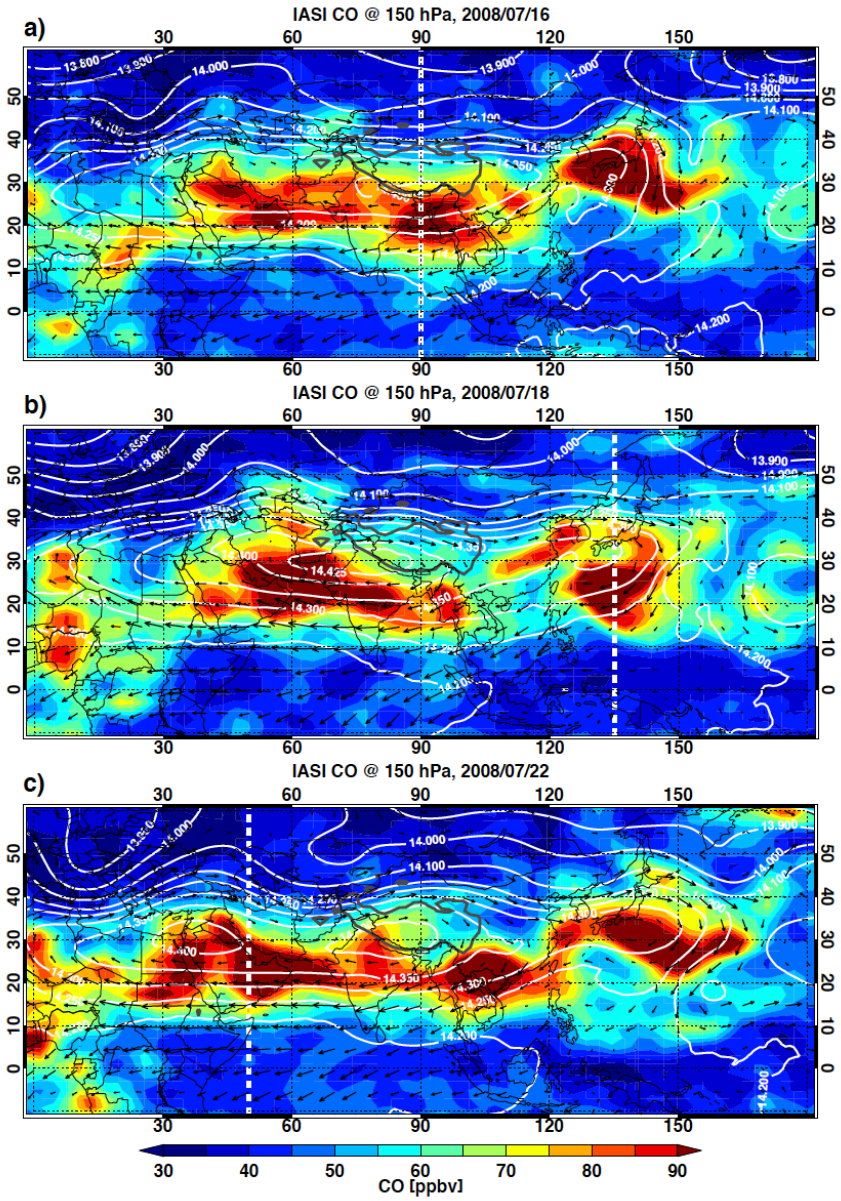

Figure 8: Same as Figure 5, but for IASI CO at 150 hPa. The maps are interpolated to 3°x2° longitude-latitude grids. The dashed white lines mark the location of the cross-sections shown in Fig. 9.

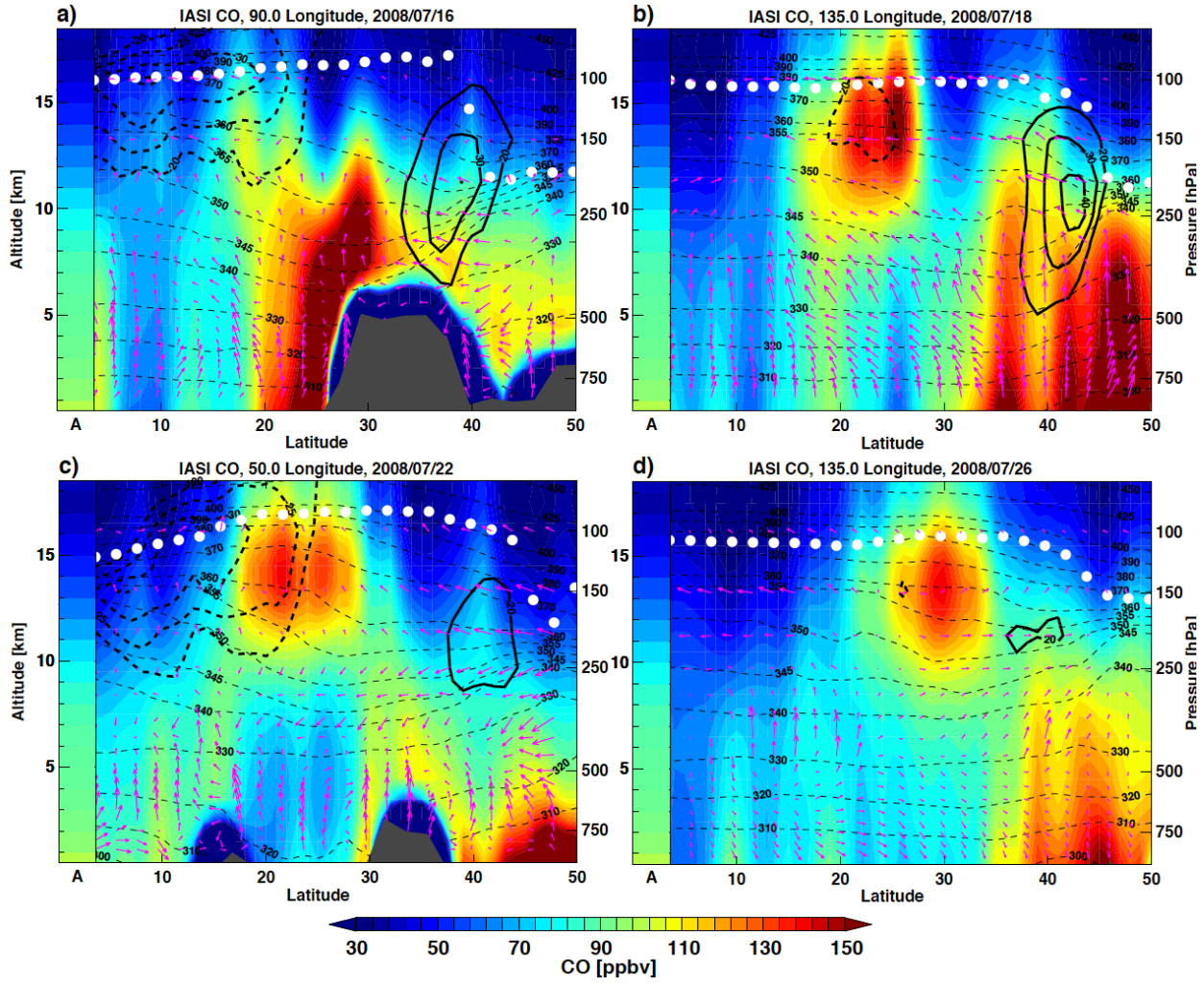

Figure 9: Selected latitude-height cross-sections of the IASI CO retrieval. The retrieval a priori profile is shown as the left-most column in each panel (marked as "A" on x-axis). The days and the location of the cross sections are selected to highlight the different vertical structures of the three modes of the anticyclone: a) 90°E on July 16 (Tibetan mode), b) 135°E on July 18 (Western Pacific mode), c) 50°E on July 22 (Iranian mode), and d) 135°E on July 27 (Western Pacific mode). The corresponding maps are given in Figures 7 and 8. A number of dynamical fields are overlaid, including zonal winds (black contours, solid (dashed) for Westley (Eastley)), meridional wind (pink arrows), potential temperatures (thin black dashed lines), and the tropopause height (white dots).

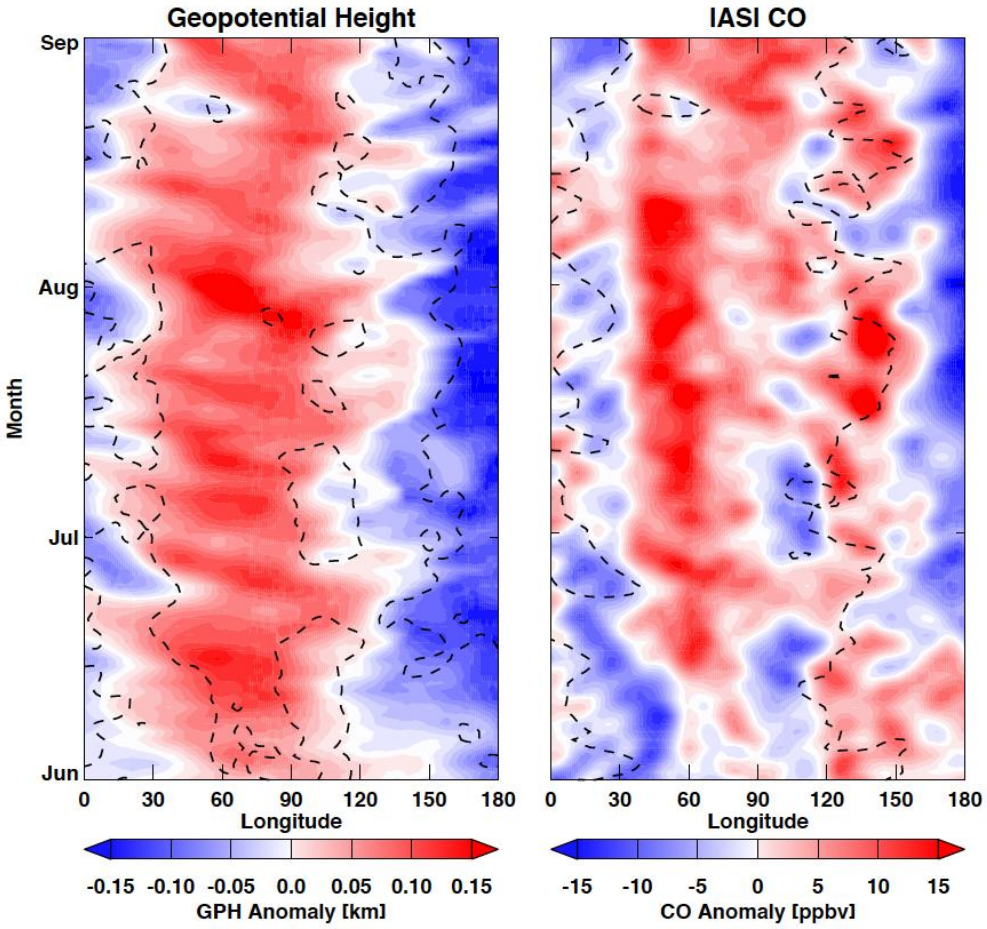

Figure 10: Same as Figure 6 but for 150 hPa IASI CO anomaly. The Pearson's correlation of the two fields for the 3-month period is 0.69.

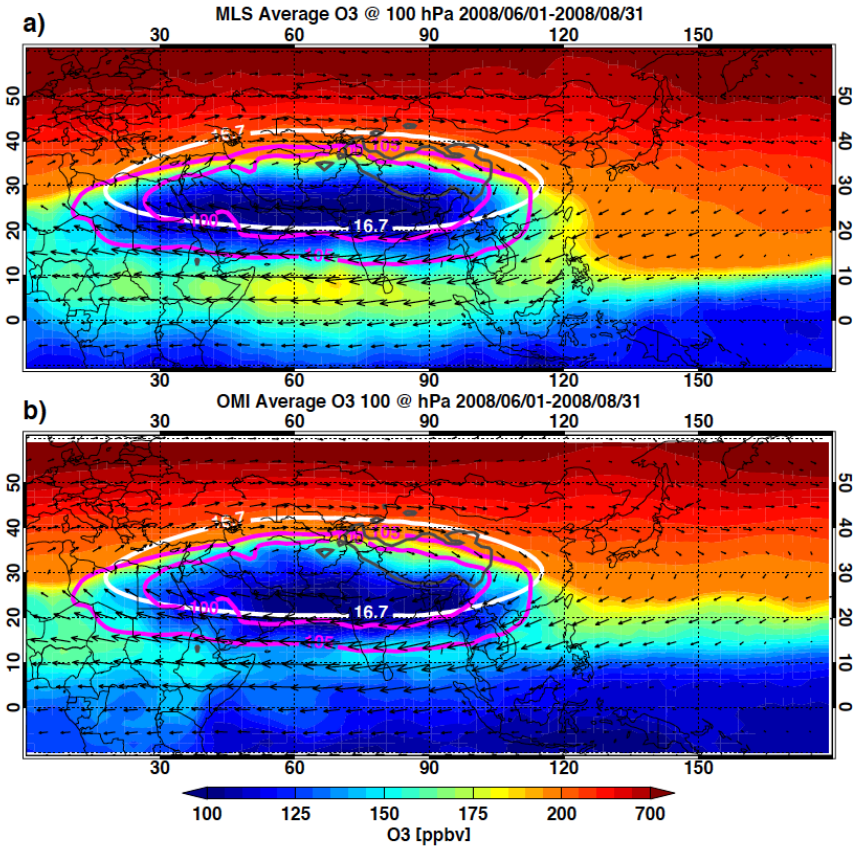

Figure 11: JJA seasonal average O_3 mixing ratio for (a) MLS and (b) OMI at 100 hPa for 2008. Superimposed white contours are the 16.7 km GPH at 100 hPa and magenta contours are the 100 and 105 hPa tropopause pressure, i.e., the ~~interception~~ intersection of the tropopause with the 100 and 105 hPa pressure surfaces. Both MLS and OMI are 2° × 2° longitude-latitude binned averages.

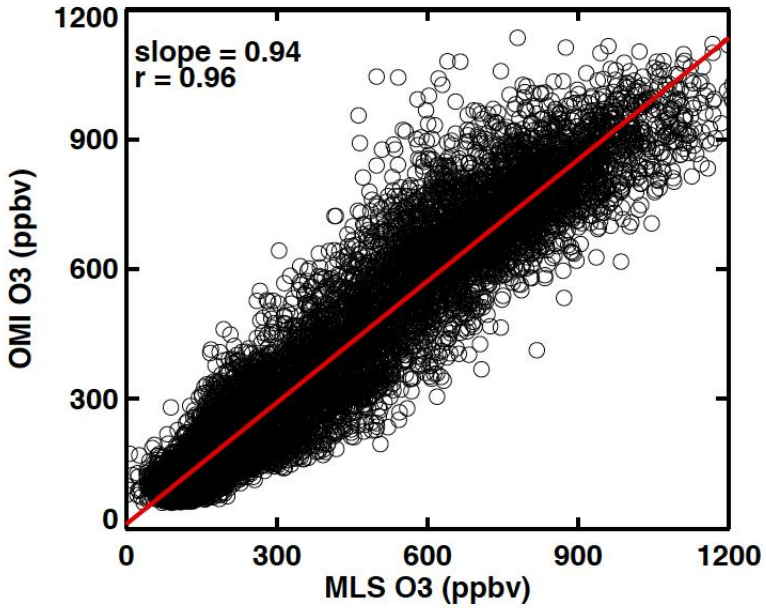

Figure 12: Same as Fig.3 but for OMI versus MLS O_3 at 100 hPa for JJA 2008. The red line shows a linear fit. Correlation and slope for the linear fit are given in the upper left corner of the panel.

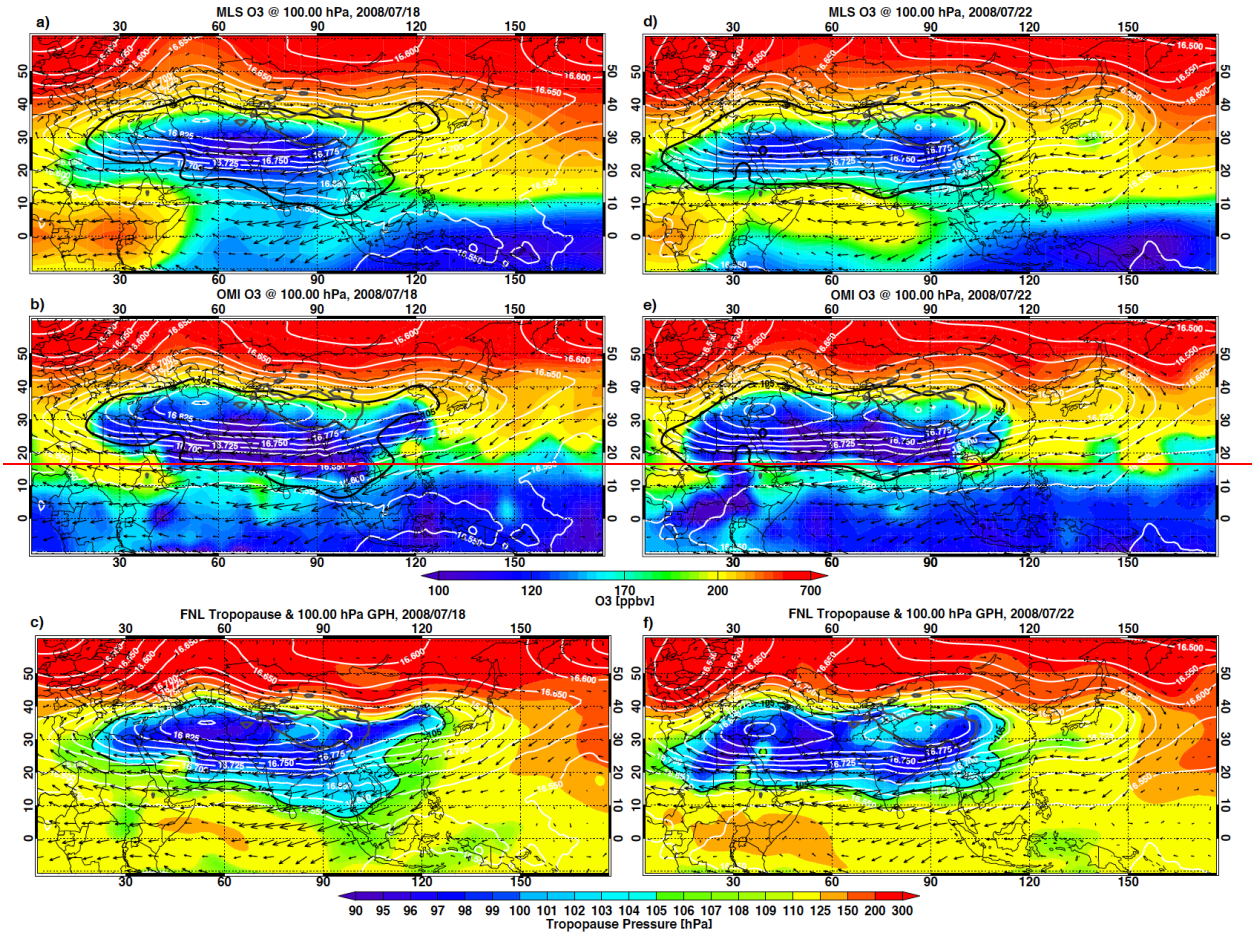
a)
MLS O3 @ 100.00 hPa, 2008/07/18
d)
MLS O3 @ 100.00 hPa, 2008/07/22
b)
OMI O3 @ 100.00 hPa, 2008/07/18
e)
OMI O3 @ 100.00 hPa, 2008/07/22
100 120 170 200 700
O3 [ppbv]
c)
FNL Tropopause & 100.00 hPa GPH, 2008/07/18
f)
FNL Tropopause & 100.00 hPa GPH, 2008/07/22
90 95 96 97 98 99 100 101 102 103 104 105 106 107 108 109 110 125 150 200 300
Tropopause Pressure [hPa]

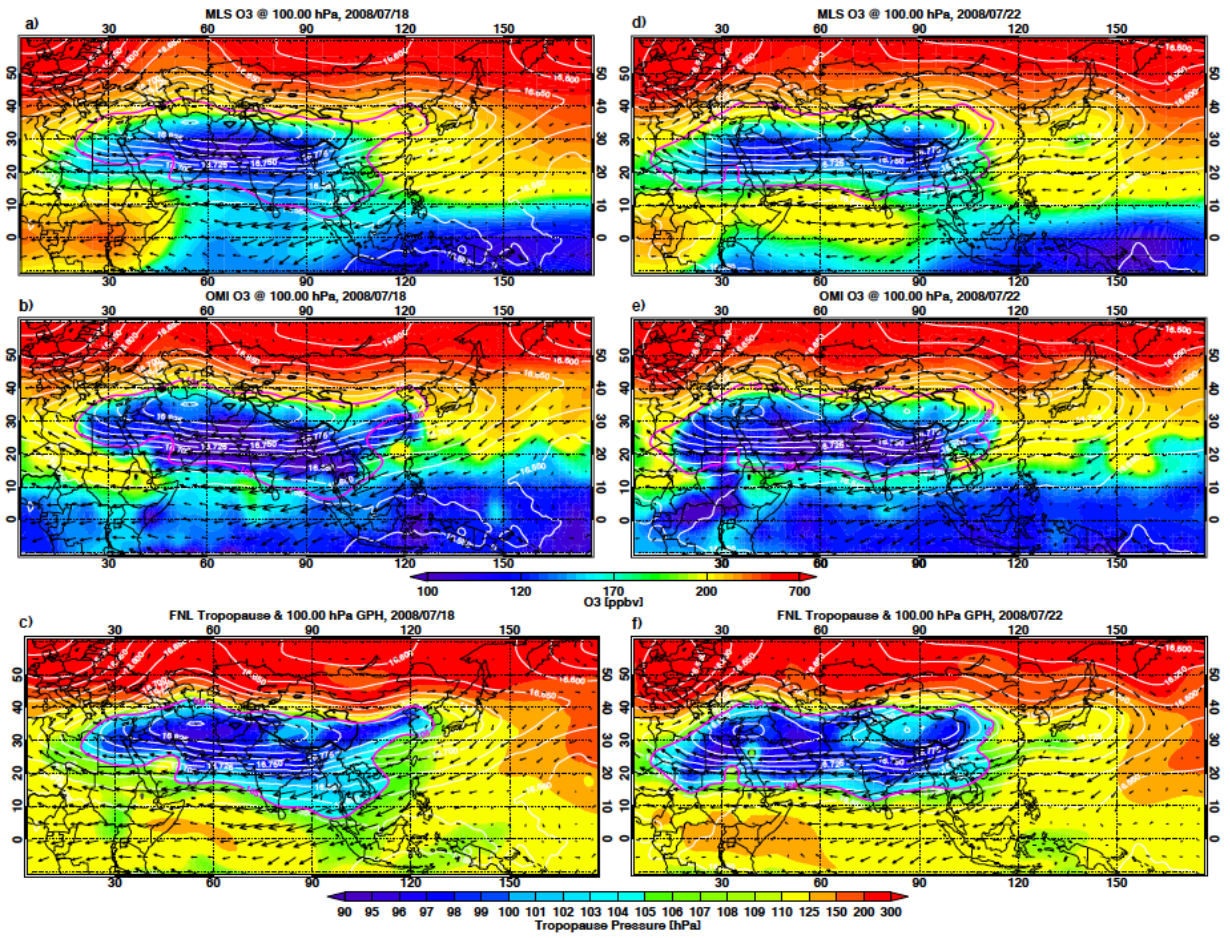

Figure 13: Daily maps of MLS and OMI O_3 mixing ratio at 100 hPa (color shading) for 18 July (a, b) and 22 July (d, e) 2008. Tropopause pressure maps for the same selected two days are in (c, f). Dynamical fields of GPH (white contours), horizontal winds (gray arrows), and 105 hPa tropopause pressure contour (pink) are superimposed. MLS maps are interpolated using natural neighbor method on 5°x5° longitude-latitude grids while OMI maps are interpolated on 1°x1° longitude-latitude grids. The tropopause pressure is from the GFS product. A Gaussian smoothing is applied to all maps. The location of the Tibetan plateau (using 3 km elevation) is also shown in the maps.

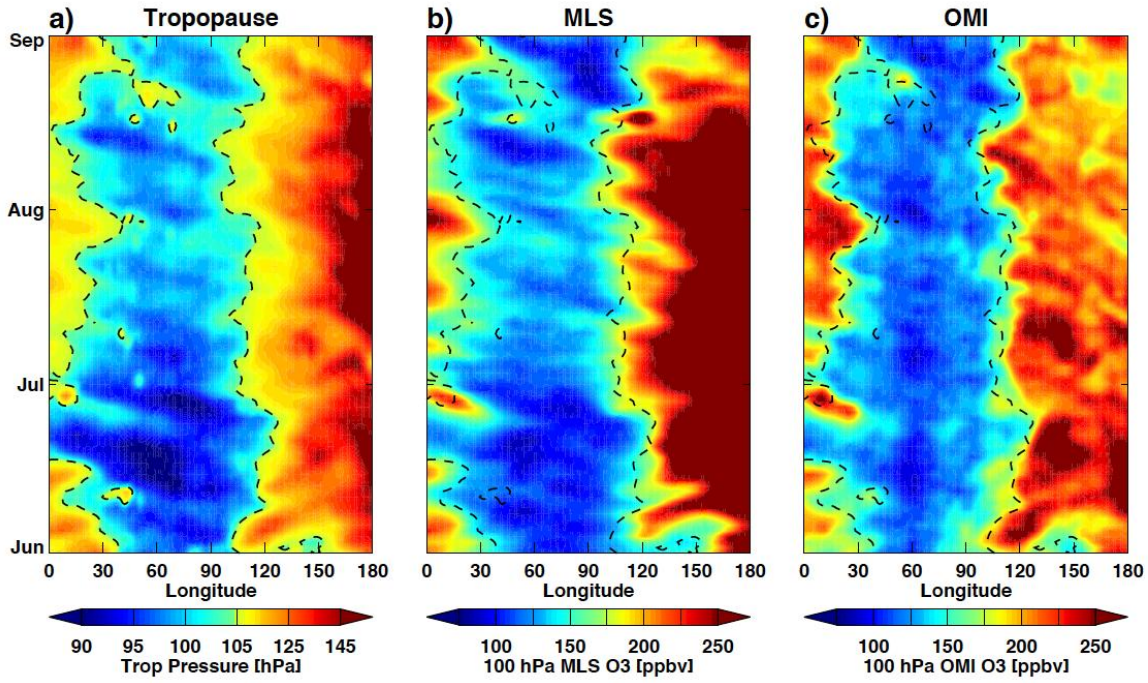

Figure 14: Longitudinal-time (Hovmöller) diagrams for (a) tropopause pressure, (b) 100 hPa MLS O_3, and (c) 100 hPa OMI O_3 for JJA season 2008. The Hovmöller diagram is constructed using daily average over 15°–35° N. MLS data has been averaged over 5° longitude bins, and OMI data averaged in 1° longitude bins. The 105 hPa zonal average tropopause pressure is shown by the dashed line on all three fields. Gaussian smoothing is applied to all three datasets.